03 Apr 1995, 11:00 am - 12:00 pm

Deformation Characteristics of Soils and Soft Rocks under Monotonic and Cyclic Loads and Their Relationships

Fumio Tatsuoka
University of Tokyo, Japan

Diego Lo Presti
Politecnico di Torino, Italy

Yukihiro Kohata
University of Tokyo, Japan

Proceedings: Third International Conference on Recent Advances in Geotechnical Earthquake Engineering and Soil Dynamics, April 2-7, 1995, Volume II, St. Louis, Missouri

Deformation Characteristics of Soils and Soft Rocks under Monotonic and Cyclic Loads and Their Relationships

Paper No. SOA1

(State of the Art Paper)

Fumio Tatsuoka
Institute of Industrial Science, University of Tokyo, Japan

Yukihiro Kohata
Institute of Industrial Science, University of Tokyo, Japan

Diego Lo Presti
Dipartimento di Ingegneria Strutturale, Politecnico di Torino, Italy

SYNOPSIS: For a wide variety of geomaterials, cohesionless and cohesive soils and sedimentary soft rocks and cement-mixed soils, the importance and advantages of measuring the deformation characteristics accurately and continuously for a strain range from less than 0.001 % to several % by a single static test using a single specimen are demonstrated. It is also shown that the deformation characteristics at strains of less than about 0.001 % is essentially elastic, and the elastic stiffness values evaluated under static (monotonic and cyclic) and dynamic (fast cyclic) loading conditions are the same from the engineering point of view. It is discussed that the plastic deformation characteristics including the damping ratio, the decay characteristics of stiffness and the liquefaction potential are not uniquely linked to the elastic properties.

INTRODUCTION

The deformation properties of geomaterials (i.e., soils and rocks) under dynamic loading conditions (i.e., relatively fast cyclic loading conditions) are an essential part of soil dynamics. In most of the previous related studies, however, the so-called "dynamic" deformation properties of geomaterials were investigated without being explicitly linked to the so-called "static" deformation properties. As Woods (1991) pointed out, it is high time to drop the modifiers "dynamic" and "static". The first rationale for the above is that apparent differences between the two types of deformation properties can be attributed to the effects of strain magnitude, strain rate, loading pattern (monotonic or cyclic) and so on, which are not exclusively related to either dynamic or static behaviour of a given mass of geomaterial. The second is that large part of the so-called "dynamic" deformation properties of a given geomaterial can be evaluated by static loading tests measuring stress(es) or load(s) and strain(s) or deformation(s), those being either monotonic or cyclic loading tests. Furthermore, large part of the so-called "static" deformation properties can be evaluated by dynamic loading tests such as wave propagation tests (e.g., ultra-sonic wave tests and bender element tests in the laboratory and field seismic surveys) and dynamic loading tests (e.g., resonant-column tests and free vibration tests) (n.b., herein, these wave propagation tests and dynamic loading tests will be called dynamic tests).

In view of the above, this report has been prepared to illustrate;
1) the importance and some advantages of measuring deformation characteristics accurately and continuously for a strain range from less than 0.001 % to several % by means of a single static test using a single specimen, and
2) the link between stiffness values evaluated under static (monotonic and cyclic) and dynamic (fast cyclic) loading conditions.
The understanding of the second point is essential to appropriately organize a systematic geotechnical investigation for a given geotechnical construction project and to establish a consistent design procedure, rather than to investigate, define and use the so-called "dynamic" and "static" deformation properties of geomaterial separately. These points have been discussed by several researchers (e.g., Jamiolkowski et al., 1991, Tatsuoka and Shibuya, 1992, Jardine, 1995, Tatsuoka and Kohata, 1995).

The strains in relatively stiff ground under working loads are in fact small, typically less than 0.5 % (e.g., Burland, 1989, Tatsuoka and Kohata, 1995), and the stiffness at these small strains evaluated by means of appropriate field and laboratory tests is one of the key parameters used to predict ground movements (e.g., Jardine et al., 1991, Jardine, 1995, Hight and Higgins, 1995, Tatsuoka and Kohata, 1995). This report will also briefly discuss the above-mentioned stiffness, which is closely linked to the so-called "dynamic" stiffness.

IMPORTANCE OF ACCURATE STRESS AND STRAIN MEASUREMENTS

Background: First of all, unless the measurements of the deformation properties of a given specimen of geomaterial in static loading tests, particularly those at small strains, are sufficiently accurate, statically determined deformation properties cannot be compared with those obtained by the corresponding dynamic tests. Herein, some important issues for accurately measuring the deformation characteristics of geomaterial in the triaxial test, rather than the torsional shear test, is herein discussed for the following two reasons;
1) the triaxial test is much more popular in geotechnical engineering practice, and
2) errors in the measured axial strains in the triaxial test can be particularly serious.

ASTM D 3999-91 "Standard Test Method for the Determination of the Modulus and Damping Properties of Soils Using the Cyclic Triaxial Apparatus" allows the measurements of axial load and axial deformation of a given specimen using transducers located outside the triaxial cell. It seems that this ASTM standard was specified for cyclic triaxial tests designed to measure the stiffness at strains larger than about 0.01 %. It is suggested in the standard to measure the stiffness at smaller strains using resonant-column tests. It has been

Table 1 Physical properties of sands from which the test results are presented in this report.

Sand	G_s	D_{50} [mm]	D_{60}/D_{10}	e_{max}	e_{min}
Toyoura	2.65	0.18	1.3	0.982	0.617 [1]
Toyoura	2.65	0.16	1.3	0.985	0.611 [2]
Ticino	2.685	0.55	1.57	0.930	0.579
Ticino+ Adda silt (Ticino silty sand)	2.680	0.51	2.32	0.744	0.470
Quiou	2.716	0.71	4.5	1.281	0.831

1) tested in Japan, 2) tested in Torino

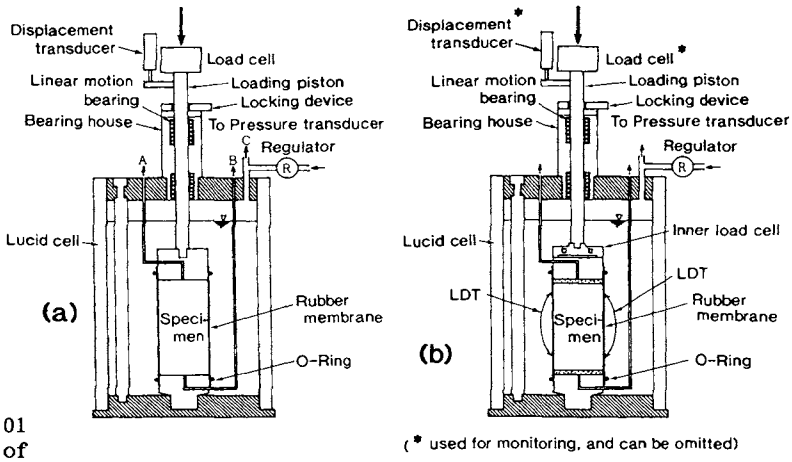

(* used for monitoring, and can be omitted)

Fig. 1 (a) Typical conventional triaxial testing system with a load cell and a displacement transducer located outside the triaxial cell and (b) a triaxial testing system with a load cell and a local axial strain gage located inside the triaxial cell used at Institute of Industrial Science (IIS), University of Tokyo.

known, however, that not only at strains larger than 0.01 %, but also at smaller strains, errors in the stiffness of geomaterials, in particular hard soils and soft rocks, evaluated by measuring axial stress and strain with transducers located outside the triaxial cells could be very large (Kokusho, 1980, Tatsuoka and Shibuya, 1992, Tatsuoka et al., 1994a, Lo Presti et al., 1994a, Toki et al., 1995, Tatsuoka and Kohata, 1995, Lo Presti, 1995).

The major potential problems encountered in the stress and strain measurements in the conventional triaxial testing system such as the one shown in **Fig. 1(a)** could be summarized as follows;
1) Due to the effects of piston friction on the measured axial load, the Young's modulus and damping ratio of a specimen, particularly the damping value, may be over-estimated (Kokusho, 1980).
2) Due to the effects of the system compliance of a test apparatus (i.e., the deformation of a loading piston, connections and so on) on the measured axial displacement, Young's modulus may be under-estimated (Kokusho, 1980). This would be particularly the case in tests using a loose connection between the loading piston and the specimen cap such as the magnetic system and the vacuum system (i.e., suction cap) described in ASTM D 3999-91.
3) Due to the effects of bedding error at the top and bottom ends of specimen on the measured axial displacement, Young's modulus may be under-estimated and the damping value may be over-estimated.
4) Due to delay in the data acquisition system for stress(es) and/or strain(s), the damping value of a specimen may be either over-estimated or under-estimated, depending on which of stress and strain is recorded in a delayed manner.

Problems 2) and 3) become more serious for stiffer geomaterials (i.e., hard soils and soft rocks).

JSSMFE standard: In view of the above, in 1991, the Japanese Society of Soil Mechanics and Foundation Engineering (JSSMFE) set up an ad hoc technical committee for "Standardization of Laboratory Cyclic Loading Test for the Determination of Deformation Properties of Geomaterials". The first and third authors of this report were, respectively, the chairman and a core member of the committee. In 1993, the committee submitted the draft of the standard for both the cyclic triaxial test using a solid cylindrical specimen and the cyclic torsional shear test using a hollow cylindrical specimen. After having been reviewed by the members of the JSSMFE, the standard was approved by the JSSMFE in 1994; i.e., JSSMFE Soil Testing Method No. JSF T 542-1994 - Method for Cyclic Triaxial Test for Deformation Properties of Geomaterials -, and No. JSF 543-1994 - Method for Cyclic Torsional Test for Deformation Properties of Geomaterials -. One of the important features of the standard is that it specifies the cyclic triaxial and torsional testing procedures used to evaluate the Young's modulus, shear modulus and damping ratio of a given single specimen continuously for a strain range from less than 0.001 % to about 1 %, while the use of resonant-column tests is not suggested.

As reported in detail by Toki et al. (1995), the JSSMFE standard specifies the cyclic triaxial testing procedure so as to avoid the four problems described above and others, in particular:
1) It is necessary to use an internal load cell placed directly above the specimen cap (i.e., inside the triaxial cell).
2) The local strain measurement along the specimen lateral surface is required using an appropriate method when the errors involved in the measured axial strains and/or damping values due to the bedding error is considered to be more than 5 % of the true value.
3) Simultaneous recording of stress and strain is required. In particular, it is necessary to evaluate the effects of the time delay in the data acquisition system for stress(es) and strain(s) before actual testing on geomaterial. It is necessary to confirm that the effects of the time delay on the damping ratio is less than 5 % when the single amplitude axial strain is about 0.01 %.

Fig. 1(b) shows a typical triaxial testing system that satisfies requirements 1) and 2) above. To substantiate the proposed standard, two round robin test programs were organized by the committee, in which Toyoura sand and sedimentary soft mudstone, respectively, were used. Toyoura sand is a uniform quartz-rich fine sand with sub-angular particles with D_{50}= 0.18 mm, U_c= 1.3, e_{min}= 0.617 and e_{max}= 0.982 (see **Table 1**). The sedimentary soft mudstone has a geological age of about 2 million years, and a large block was obtained from a depth of 50 m at a site near Tokyo. The results of the two round robin test programs were analysed by, respectively, Dr. Yamashita, S. of Kitami Institute of Technology and the third author of this report. Herein reported is part of the result obtained from these round robin test programs and those obtained from other tests performed by the authors and their colleagues which supplements the former.

Results for Toyoura sand: Part of the results for dense Toyoura sand obtained from the round robin test program

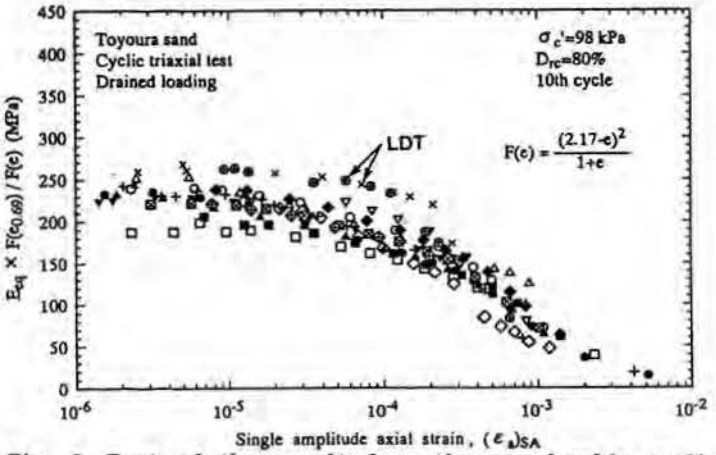

Fig. 2 Part of the result from the round-robin cyclic triaxial test program using Toyoura sand organized by JSSMFE; comparison of $E_{eq} \sim \log(\varepsilon_a)_{SA}$ relations obtained from 15 tests (Fig. 3-3b of Toki et al., 1994).

are shown in **Fig. 2**. The complete results are reported in Toki et al. (1995). In total, seventeen different laboratories in Japan joined this program using Toyoura sand. The definitions of the Young's modulus and the other related parameters used in this report are given in **Fig. 3**. For the data shown in Fig. 2, the void ratio and the relative density D_r after consolidation ranged between 0.657 and 0.701 and between 77 % and 89 %, respectively. The Young's moduli have been corrected to those at a void ratio of 0.69 (i.e., D_r= 80 %) based on the empirical function; $F(e) = (2.17 - e)^2/(1 + e)$ (Hardin and Richart, 1963, Iwasaki et al., 1978).

The specimens were prepared by following the same procedure (i.e., pluviation of air-dried particles from a nozzle with a constant fall height). The top end of each specimen was finished by scraping with a straight edge so as to obtain a flat surface in parallel to the cap face. The top and bottom ends of the specimen were placed in contact with a porous stone disk without using filter paper. In Fig. 2, the results of fifteen tests are shown. For one test (i.e., the data points ▼), the specimen was 30 cm in diameter (D) and 60 cm in height (H), while for the other tests, the specimen dimensions ranged from 5 cm to 7.5 cm in D, from 10 cm to 17 cm in H and from 2.0 to 2.4 in H/D. After having been saturated, the specimens were isotropically consolidated to σ'_c= 98 kPa. In most of the tests, at each loading stage with a constant cyclic stress amplitude, ten cycles of symmetrical sinusoidal cyclic deviator stresses were applied at a frequency ranging from 0.05 Hz and 0.5 Hz (mostly 0.1 Hz) under drained conditions (n.b., undrained tests were also performed, the results of which are reported in Toki et al., 1995). In the other two tests, symmetric sinusoidal cyclic axial strains were used. The data obtained at the tenth cycle at each loading stage were analysed.

The main difference in the testing procedures for these tests existed in the method of axial strain measurement. In thirteen tests, axial strains were obtained only from the axial displacement of the specimen cap measured with either a couple of proximity transducers (ten tests) and LVDTs (three tests) placed diametrically opposite each other, while in the other two tests, the axial strains were measured locally by using a pair of LDT (Local Deformation Transducer, Goto et al., 1991; see Fig. 1b). It may be seen from Fig. 2 that the Young's moduli obtained based on locally measured axial strains in the two tests are very similar to each other, and for strains of less than about 0.02 %, they are larger than those obtained based on

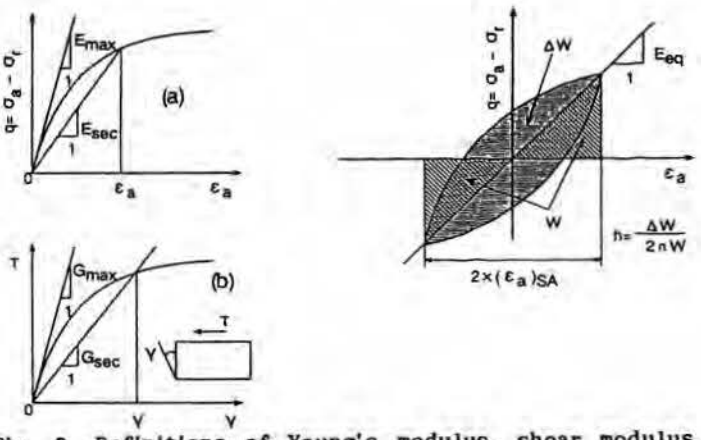

Fig. 3 Definitions of Young's modulus, shear modulus, single amplitude strain and damping ratio

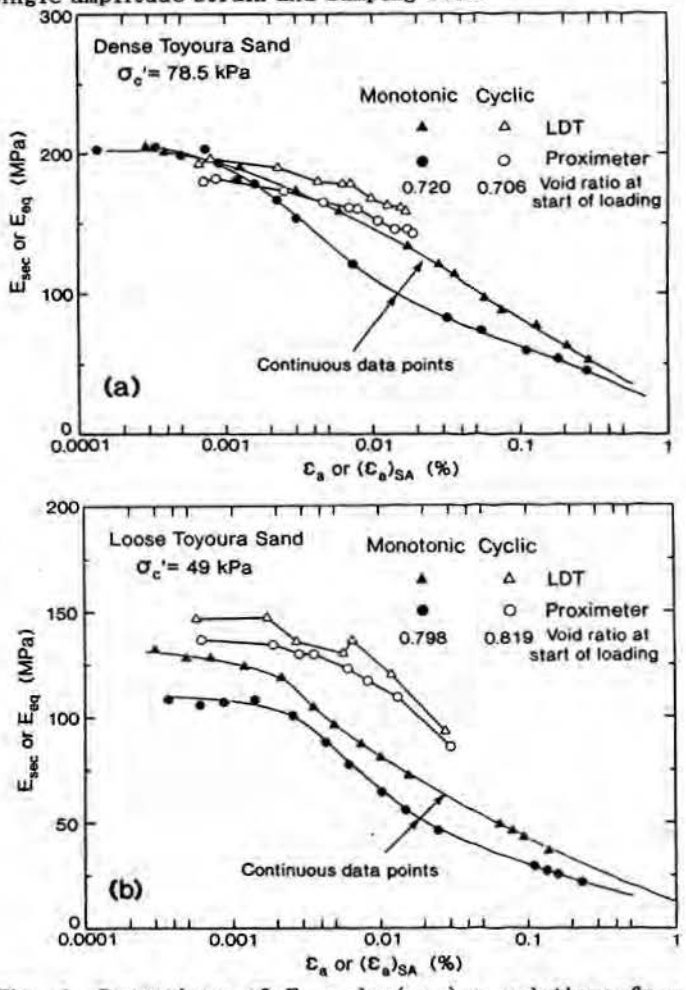

Fig. 4 Comparison of $E_{eq} \sim \log(\varepsilon_a)_{SA}$ relations from a cyclic loading triaxial test with $E_{sec} \sim \log \varepsilon_a$ relations from a monotonic loading test, D= 7.5 cm and H= 15 cm, air-dried Toyoura sand; a) dense and b) loose (Teachavorasinskun, 1992, Tatsuoka et al., 1994a)

externally measured axial strains. The authors consider that the difference is due to the effects of the bedding error. In addition, the scatter in the data obtained from external strain measurements is not very small.

The effect of the bedding error can be better quantified in the results of a single test in which axial strains are measured both locally and externally, as shown in **Fig. 4**.

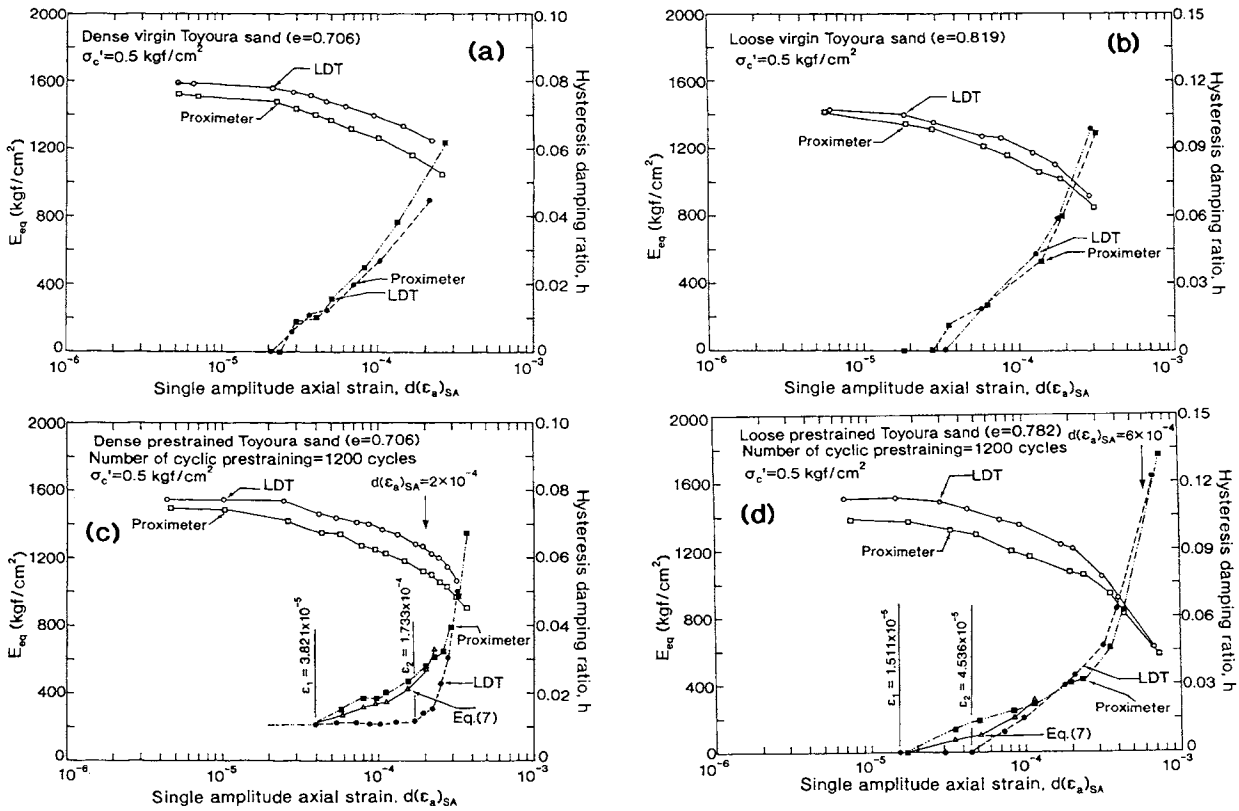

Fig. 5 E_{eq} and $h \sim \log(\varepsilon_a)_{SA}$ relations from cyclic loading triaxial tests on air-dried Toyoura sand, σ_c' = 49 kPa; a) dense virgin, b) loose virgin, c) cyclically prestrained dense, and d) cyclically prestrained loose; "proximeter" stands for external axial strains obtained from the axial displacement of the specimen cap; the void ratios are those measured at the start of each cyclic loading series (Teachavorasinskun, 1992, Kohata et al., 1993).

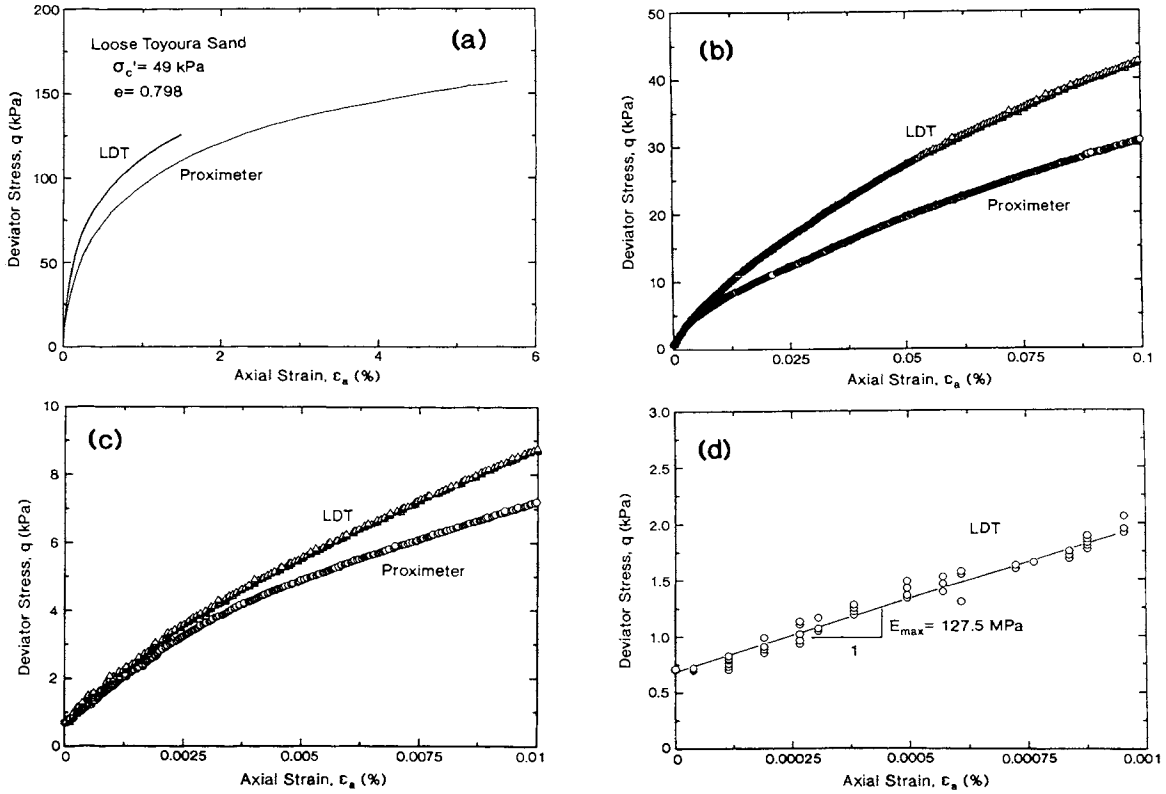

Fig. 6 A typical result of CD triaxial compression test on air-pluviated loose Toyoura sand (Teachavorasinskun, 1992).

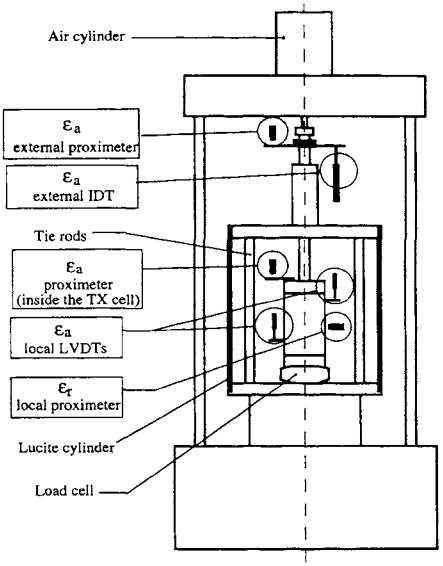

Fig. 7 Triaxial testing system with a load cell and a local axial strain gage located inside the triaxial cell in Italy (Lo Presti et al., 1994a and 1994b, Jamiolkowski et al., 1994, Fioravante et al., 1993, Pallara 1995).

Table 2 Specifications of a triaxial testing system with a load cell and a local axial strain gage located inside the triaxial cell used in Italy, see Fig. 7 (Lo Presti et al., 1994a and 1994b, Jamiolkowski et al., 1994, Fioravante et al., 1993, Pallara 1995).

Gauge	Resolution(microns)	Accuracy(microns)	Capacity(mm)
Submersible LVDT	0.3	1	2
Proximity transducer	0.3	1	2.5
IDT	5	20	20

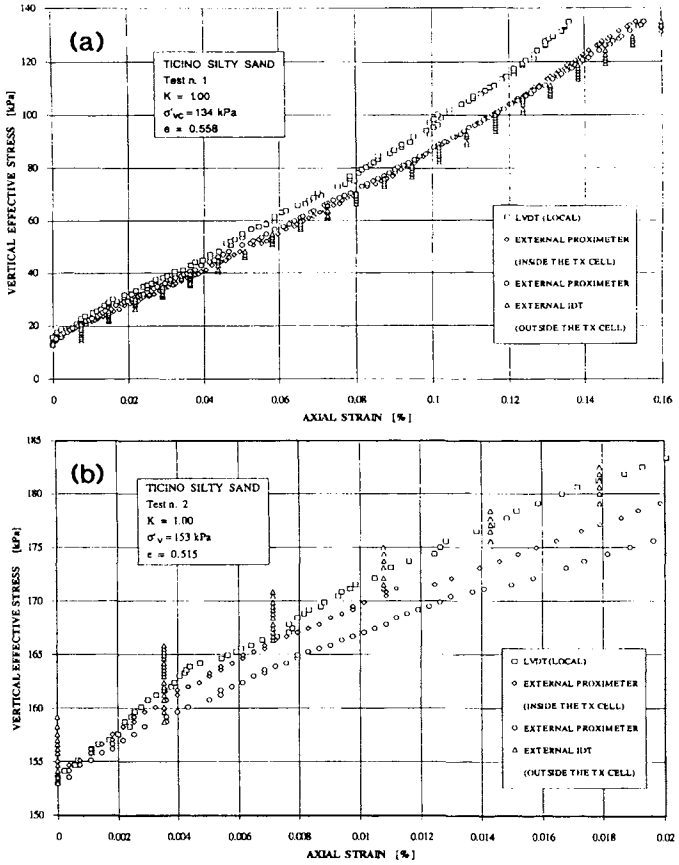

Fig. 8 A typical test result of air-pluviated Ticino silty sand; a) isotropic consolidation stage, and b) CD triaxial compression test stage (Lo Presti, 1994a).

In these cyclic triaxial tests, air-dried dense and loose Toyoura sand were tested at σ_c' = 78.5 kPa under otherwise the same testing conditions as the round robin test program (n.b., a comparison with the results of monotonic loading tests shown in these figures is made in the later part). **Fig. 5** also shows the results of similar tests on Toyoura sand. For the data shown in Fig. 5, a specimen of Toyoura sand was prepared using the air-pluviation method, and the E_{eq} and $h \sim (\varepsilon_a)_{SA}$ relations were obtained first by following the JSSMFE standard (Figs. 5a and b). Then, at the strain levels $(\varepsilon_a)_{SA}$ designated by the symbol ↓ in Figs. 5(c) and (d), 1,200 cycles of symmetrical cyclic deviator stress were applied. The relationships between E_{eq}, h and $(\varepsilon_a)_{SA}$ were then again obtained (Figs. 5c and d) (n.b., the damping ratio h and the effects of cyclical prestraining on E_{eq} and h is later discussed). It may be seen from these figures that even in cyclic triaxial tests on such a fine sand, the effects of the bedding error are consistently noticeable.

The effects of the bedding error is generally larger in monotonic loading (ML) triaxial compression test. **Fig. 6** shows stress-strain relations obtained from a typical ML triaxial compression test on air-pluviated loose Toyoura sand (Teachavorasinskun, 1992). The sample was 7.5 cm D and 15 cm H, and the top and bottom ends of the specimen were in contact with the porous stone fixed to the cap and the pedestal. Large effects of the bedding error can be noticed except at the very beginning stage of test.

At Politecnico di Torino (Technical University of Torino), the axial strain is measured both externally and locally in triaxial compression tests on sand (**Fig. 7**). External axial strains are obtained by using a) a high-resolution proximity transducer and a conventional inductance displacement transducer (IDT), both of which measure the axial displacement of the loading piston outside the triaxial cell, and b) a high-resolution proximity transducer located inside the triaxial cell, which measures the axial displacement of the specimen cap. Local axial strains are obtained by using a pair of high-resolution submergible LVDTs, which measure the axial compression of the central zone of the specimen. The axial load is measured with an internal load cell with a capacity of 10 kN and a resolution of 0.064 N, which is commercially available. This load cell is very rigid, submergible and insensitive to the change in hydro-static pressure. The radial strain is measured locally by using a pair of proximity transducers located at the specimen mid-height.

Fig. 8 show a typical result obtained for a) isotropic consolidation stage and b) ML drained triaxial compression stage at σ_c' = 160 kPa using Ticino silty sand with a fines content of 11.6 % and D_r = 77.2 % (Table 1). The sample was 7.1 cm in D and 14.2 cm in H and the axial strain rate was 0.01 %/min. It may be seen that local axial strains measured along the lateral surface of specimen with a pair of LVDTs are consistently smaller than those measured externally. It is also to be noted that the resolution of the IDT is too low to detect small axial strains. A resolution much less than 1 μm, which is equivalent to an axial strain 0.001 %, is necessary to measure reliably axial strains of 0.001 % for a gage length of 10 cm.

Fig. 9 shows the ratio of E_{sec} values based on locally and

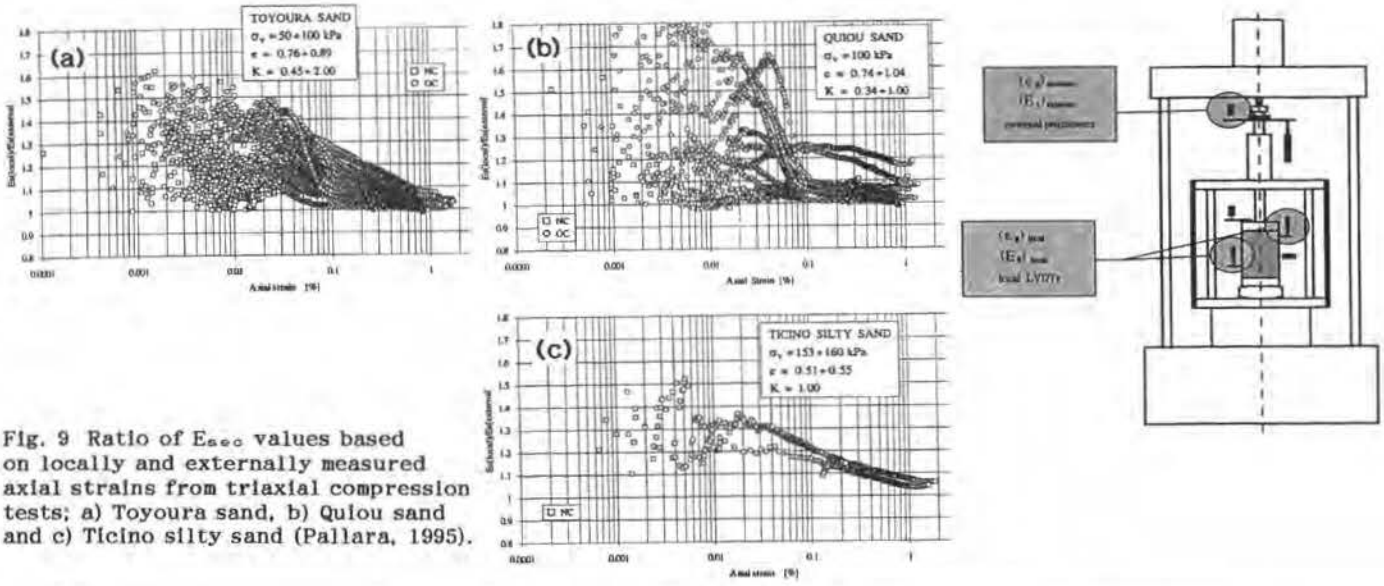

Fig. 9 Ratio of E_{sec} values based on locally and externally measured axial strains from triaxial compression tests; a) Toyoura sand, b) Quiou sand and c) Ticino silty sand (Pallara, 1995).

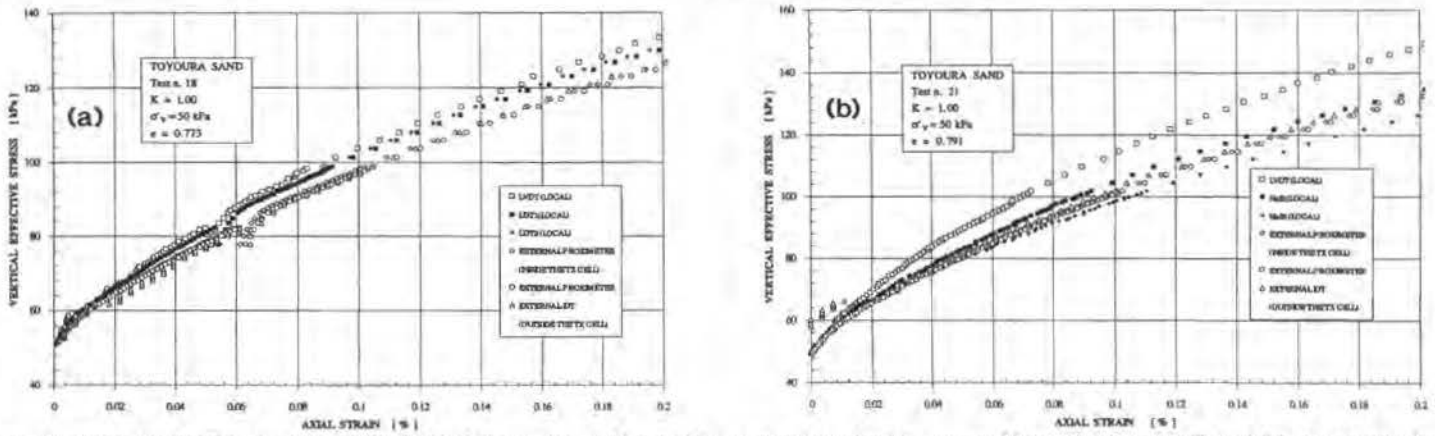

Fig. 10 Typical test results of CD triaxial compression tests on isotropically consolidated air-pluviated Toyoura sand; a) test No. 18, and b) test No.21 (Lo Presti et al., 1994a, Lo Presti, 1995, Jamiolkowski et al., 1994, Fioravante et al., 1993, Pallara 1995).

externally measured axial strains as a function of axial strain obtained from the following three series of triaxial compression tests on sands; a) 39 tests on Toyoura sand (Lo Presti et al., 1995, Pallara 1995, Jamiolkowski et al., 1994, Lo Presti et al., 1994b), b) 14 tests on Quiou sand (Fioravante et al., 1993, Pallara 1995, Lo Presti et al., 1995), and c) 3 tests on Ticino silty sand (Lo Presti et al., 1994a). The following trends may be noted:

1) Among the three types of sands, some difference in the bedding error effects can be noted, but generally, the scatter of the data is not systematic.
2) The largest ratio is as large as 1.8.
3) The ratio is not constant even in a single test, but changes with strain; generally, the ratio decreases with strain.

These results mean that the precise correction of externally measured axial strains for the bedding error effects is not feasible.

The result of a systematic comparison of the results obtained by using different local strain gages set along the lateral surface of a Toyoura sand specimen is shown in **Fig. 10**. In the test for Fig. 10a, the straining was ceased for about 30 minutes at an axial strain of about 0.05 % to examine the creep deformation of Toyoura sand. This point is not discussed here. The local gages are; a) a pair of LVDTs (Fig. 7), a pair of LDTs (Fig. 1b), and a pair of Hall Effect Transducers (Clayton and Khatrush 1986). It may be seen that the local axial strains measured with LVDTs and LDTs are very similar to each other, while they are smaller than those measured externally. In this case, the measurement with a local gage based on Hall effects was found unreliable, perhaps due to the effects of the system compliance of the device which fixes the gauge on the surface of the specimen.

Fig. 11 shows the relationship between the coefficient of hysteretic damping (or damping ratio) h and the single amplitude axial strain $(\varepsilon_a)_{SA}$, corresponding to Fig. 2. The effects of the different strain measuring methods is not discernible. However, the effect is noticeable when compared for a single test (Fig. 5), in particular when the damping ratio is very small, for example, after the application of cyclic pre-straining as shown in Figs. 5(c) and (d). It may be seen from Figs. 5(c) and (d) that even after the application of cyclic prestraining, the effects of bedding error are noticeable on the E_{sec} values, but the effects are also remarked on the h values, in particular for the dense sand (Fig. 5c). Note that in these figures, as the h values are plotted against either locally or externally measured axial strains, the difference between the h values is less discernible than they actually are.
Pairs of h values based on locally and externally measured axial strains measured at each loading stage ob-

tained from these tests are compared in **Fig. 12.** It may be seen that even for reconstituted specimens of such a fine sand, the local axial strain measurements is imperative to accurately estimate the damping values, particularly small values.

Attempts have been made to theoretically explain this difference in the values of h (Teachavorasinskun, 1992, Kohata and Tatsuoka, 1993). First, it is assumed that a thin loose layer with a thickness of **a**·H/2 exists at both the top and bottom ends of a sand specimen (**Fig. 13**; H is the height of the specimen). Fig. 13(b) shows schematically **A**) the assumed local stress-strain relation in the end looser layers, which cannot be measured, **B**) the local relation for the central part of the specimen, which is measured with LDTs, and **C**) the average relation, which is measured with an external gage. With the single amplitude external axial strain $(d\varepsilon_{a\text{-}ave})_{SA}$ and the single amplitude deviator stress q_{SA}, the equivalent Young's modulus for the average relation is obtained as;

$$(E_{eq})_{ave} = q_{SA}/(d\varepsilon_{a\text{-}ave})_{SA} \qquad (1)$$

The average strain consists of local strains in the thin looser layers and the central zone, $(d\varepsilon_{a\text{-}A})_{SA}$ and $(d\varepsilon_{a\text{-}B})_{SA}$, as;

$$\begin{aligned}(d\varepsilon_{a\text{-}ave})_{SA} &= \mathbf{a}\cdot(d\varepsilon_{a\text{-}A})_{SA} + (1-\mathbf{a})\cdot(d\varepsilon_{a\text{-}B})_{SA} \\ &= \mathbf{a}\cdot\{q_{SA}/(E_{eq})_A\} + (1-\mathbf{a})\cdot\{q_{SA}/(E_{eq})_B\} \qquad (2)\end{aligned}$$

From Eqs. (1) and (2), we obtain;

$$(E_{eq})_{ave} = (E_{eq})_B/\{(\mathbf{a}\cdot X + (1-\mathbf{a})\} \qquad (3a)$$

where,

$$X = (E_{eq})_B/(E_{eq})_A = (d\varepsilon_{a\text{-}A})_{SA}/(d\varepsilon_{a\text{-}B})_{SA} \qquad (3b)$$

The average dissipated energy per cycle for unit volume is obtained as:

$$\Delta W_{ave} = \mathbf{a}\cdot\Delta W_A + (1-\mathbf{a})\cdot\Delta W_B \qquad (4)$$

where ΔW_A and ΔW_B are the values of ΔW for, respectively, the end looser thin layers and the central part of the specimen. By definition, the coefficients of hysteretic damping ratio for these two parts, h_A and h_B, are obtained as ;

$$h_A = \Delta W_A/(2\pi W_A), \quad W_A = (d\varepsilon_{a\text{-}A})_{SA}\cdot q_{SA} \qquad (5a)$$
$$h_B = \Delta W_B/(2\pi W_B), \quad W_B = (d\varepsilon_{a\text{-}B})_{SA}\cdot q_{SA} \qquad (5b)$$

From Eq. (2), we obtain;

$$W_{ave} = \mathbf{a}\cdot W_A + (1-\mathbf{a})\cdot W_B \qquad (6)$$

Then, the average value h_{ave} for the whole specimen is obtained from Eqs. (3), (4), (5) and (6) as;

$$\begin{aligned}h_{ave} &= \Delta W_{ave}/(2\pi W_{ave}) \\ &= \{\mathbf{a}\cdot X\cdot h_A + (1-\mathbf{a})\cdot h_B\}/\{\mathbf{a}\cdot X + (1-\mathbf{a})\} \qquad (7)\end{aligned}$$

To obtain the value of h_{ave} for a measured value of h_B, the unknown parameters in Eq. (7), the values of **a**, h_A and X, should be determined, whereas they cannot be measured. These values can be estimated as follows. In the data shown in Figs. 5 (c) and (d), the value of h_B based on axial strains locally measured with LDTs starts to increase at a strain designated by ε_2, while the value of h_{ave} based on average axial strains measured externally with proximeters starts to increase at a strain designated by ε_1. It is assumed that at the loading stage where the average strain ε_1 is measured, the local strain $(d\varepsilon_{a\text{-}A})_{SA}$* in the end looser thin layers is equal to ε_2. Then, we obtain from Eq. (2);

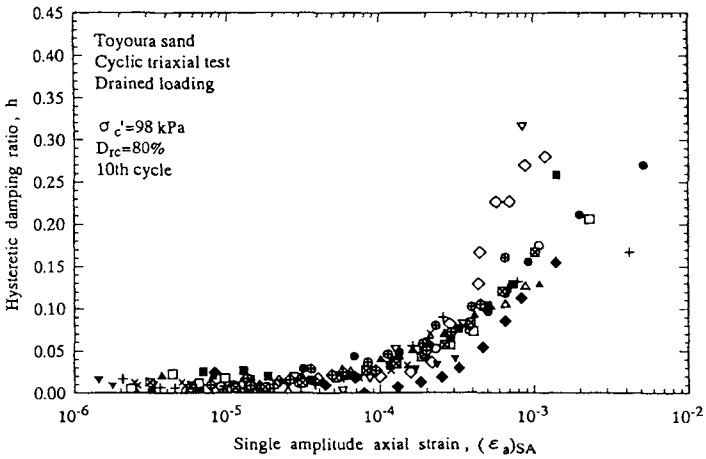

Fig. 11 Part of the result from the round-robin cyclic triaxial test program using Toyoura sand organized by JSSMFE; comparison of h~log(ε_a)$_{SA}$, corresponding to Fig. 2 (Fig. 3-6b of Toki et al., 1994).

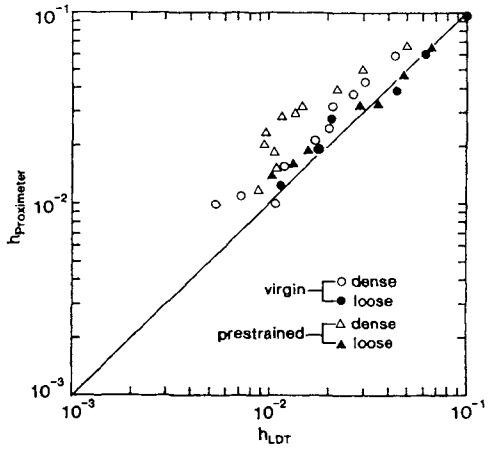

Fig. 12 Comparison between the values of h based on locally and externally measured axial strains, Toyoura sand; see Fig. 5 (Kohata et al., 1994b, Tatsuoka et al., 1994a).

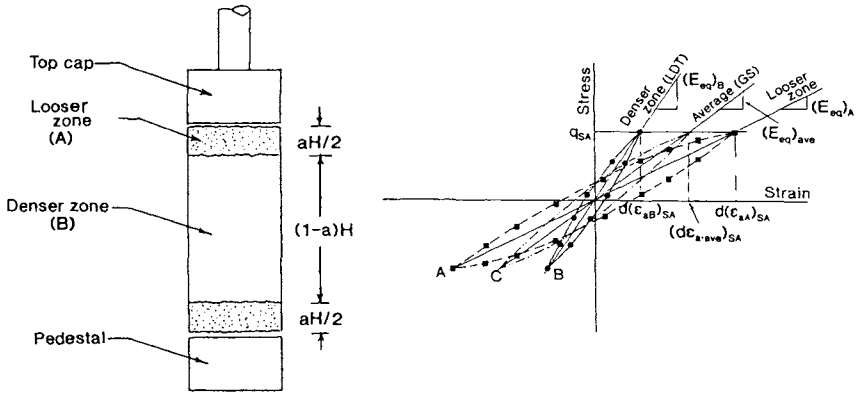

Fig. 13 Schematic figures explaining a) thin loose layers at the top and bottom of sand specimen, and b) two local stress-strain relations in the end looser layers and the central part of a sand specimen and the average stress-strain relation (the figures are not to scale).

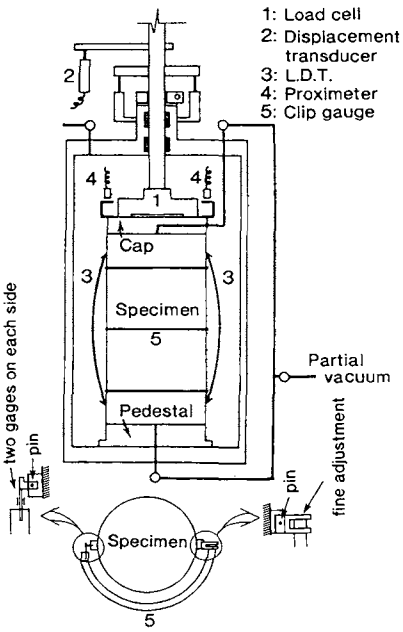

Fig. 14 Large triaxial testing apparatus with a local strain measuring system (Tatsuoka et al., 1994a)

$$\varepsilon_1 = \mathbf{a}^* \cdot \varepsilon_2 + (1 - \mathbf{a}^*) \cdot (d\varepsilon_{a \cdot B})_{SA}^* \qquad (8a)$$

$$\mathbf{a}^* = \{\varepsilon_1 - (d\varepsilon_{a \cdot B})_{SA}\} / \{\varepsilon_2 - (d\varepsilon_{a \cdot B})_{SA}^*\} \qquad (8b)$$

where $(d\varepsilon_{a \cdot B})_{SA}^*$ is the value measured at the loading stage where ε_1 is measured. At the loading stage where the value of ε_1 was measured for the case of Figs. 5(c) and (d), we obtain $\mathbf{a}^* = 0.023$ and 0.051, respectively. Then, with $(d\varepsilon_{a \cdot A})_{SA} = \varepsilon_2$, we obtain by using Eq. (8);

$$X = (d\varepsilon_{a \cdot A})_{SA}^* / (d\varepsilon_{a \cdot B})_{SA}^* = \varepsilon_2 / (d\varepsilon_{a \cdot B})_{SA}^* = \{\varepsilon_2 \cdot (1 - \mathbf{a}^*)\} / \{\varepsilon_1 - \mathbf{a}^* \cdot \varepsilon_2\} \qquad (9)$$

It is assumed that the value X is independent of the strain level. This assumption is perhaps an approximated one. On the other hand, from Eq. 3(a), for a loading stage where $(E_{eq})_B$ and $(E_{eq})_{ave}$ are measured, we obtain the parameter **a** at this loading stage as;

$$\mathbf{a} = \{(E_{eq})_B / (E_{eq})_{ave} - 1\} / (X - 1) \qquad (10)$$

Then, the theoretical value of h_A at this loading stage, where a certain value of $(d\varepsilon_{a \cdot B})_{SA}$ is measured, is equal to the value of h_B (based on LDT measurements) corresponding to $(d\varepsilon_{a \cdot A})_{SA} = X \cdot (d\varepsilon_{a \cdot B})_{SA}$. The value of h_A can be obtained from the $h_B \sim (d\varepsilon_{a \cdot B})_{SA}$ relation as shown in Fig. 5.

With a given set of the measured values of h_B, $(d\varepsilon_{a \cdot B})_{SA}$, $(E_{eq})_B$, $(d\varepsilon_{a \cdot ave})_{SA}$ and $(E_{eq})_{ave}$ for a certain loading stage and by using the values of X (Eq. 9), **a** (Eq. 10) and h_A (as obtained by the method shown above), we can obtain the theoretical value of h_{ave} based on Eq. (7) for the measured value of $(d\varepsilon_{a \cdot ave})_{SA}$. The theoretical relationship between h_{ave} and $(d\varepsilon_{a \cdot ave})_{SA}$ is shown in Figs. 5(c) and (d) as designated by "Eq. (7)". It is seen that each theoretical relation is similar to the corresponding measured relationship designated by "proximeter". Now the large difference in the h values based on locally and externally measured axial strains seen for the cyclically pre-strained dense specimen (Fig. 5c) is now explained by the fact that the h value based on locally measured axial strains suddenly start to increase

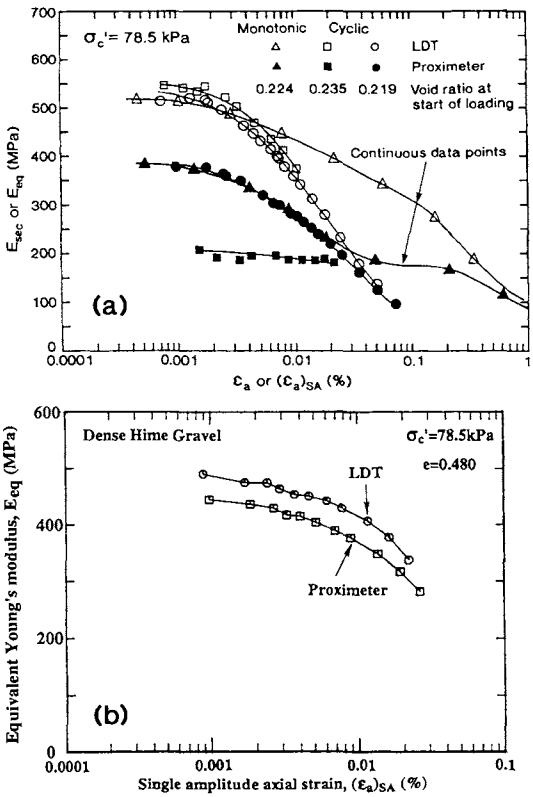

Fig. 15 a) $E_{eq} \sim \log(\varepsilon_a)_{SA}$ relations from two cyclic triaxial tests and $E_{sec} \sim \log \varepsilon_a$ relations from a monotonic loading triaxial compression test, dense Nagoya gravel, and b) $E_{eq} \sim \log(\varepsilon_a)_{SA}$ relations from a cyclic triaxial test, dense Hime gravel; specimen dimensions, D= 30 cm and H= 60 cm (Tatsuoka et al., 1994a, Dong et al., 1994).

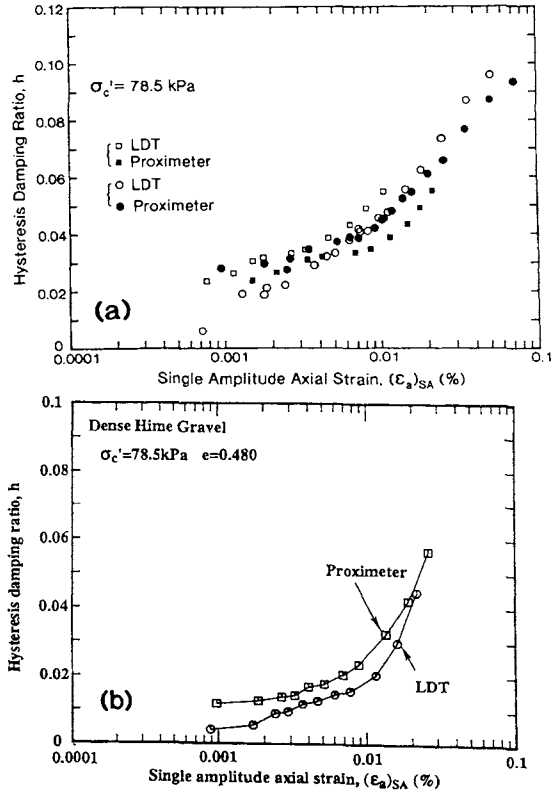

Fig. 16 $h \sim \log(\varepsilon_a)_{SA}$ relations from two cyclic triaxial tests; a) dense Nagoya gravel and b) dense Hime gravel (Dong et al., 1994).

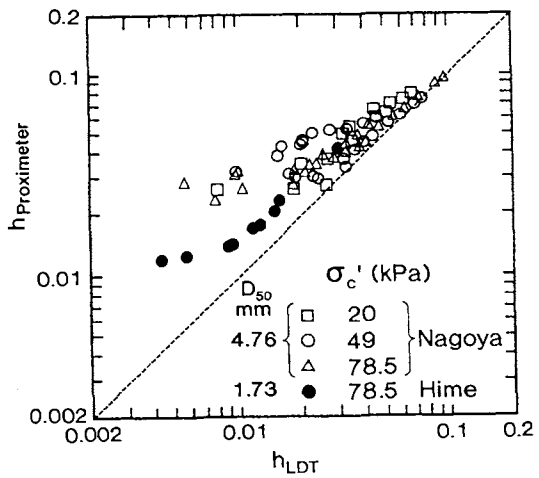

Fig. 17 Comparison between the values of h based on locally and externally measured axial strains, Nagoya and Hime gravels (Dong et al., 1994).

at a certain strain level (i.e., ε_a) and subsequently increases at a high rate with the increase in strain.

The effects of the bedding error on the values of E_{eq} and h in cyclic triaxial tests generally become more serious as the grain size becomes larger (being more serious for gravels than for fine sands) and for undisturbed stiff soils than for reconstituted soils (Tatsuoka and Shibuya, 1992 and Tatsuoka and Kohata, 1995). Tatsuoka et al. (1994a) and Dong et al. (1994) reported the results of a series of cyclic triaxial tests on dense air-dried samples of a well-graded crushed sandstone (Nagoya gravel with D_{50}= 4.76 mm, U_c= 91.8 and sub-angular particles) and a poorly-graded river gravel (Hime gravel with D_{50}= 1.73 mm, U_c= 1.33 and sub-round particles). The cyclic loading procedures followed the JSSMFE standard. The samples were 30 cm in diameter and 60 cm high, and a large triaxial testing apparatus with a local strain measuring system was used (**Fig. 14**). **Fig. 15** shows typical $E_{eq} \sim \log(\varepsilon_a)_{SA}$ relations obtained from these tests. Large effects of the bedding error may be seen, particularly for well-graded Nagoya gravel. Corresponding to the above, the effects of the bedding error on the damping ratio h were also noticeable (**Figs. 16** and **17**). The result of a CD triaxial compression test is also shown in Fig. 15a. It is seen that the effect of the bedding error is also considerable in the ML test.

All the test results available to the authors show that even in triaxial tests on fine sand may involve noticeable errors in externally measured axial strains, the amount of which is not stable (i.e., not repeatable and reproducible). The authors suggest to use an appropriate axial strain gage even in triaxial tests on most types of fine sands if the purpose of the test is to accurately evaluate the deformation characteristics at very small to small strains. The use of a local gage is a must in triaxial tests using a lubricated ends in most cases. These points should be emphasized although it is very painful for an experimentalist to modify the testing procedure which he or she has been using for a long time.

Results for sedimentary soft mudstone: Five different Japanese laboratories joined the round robin test program using sedimentary soft rock. Core samples of 5 cm in D and 10 cm in H (with one exception of 15 cm in H) were obtained by rotary coring using a diamond core barrel in the laboratory from a single large block obtained in a tunnel at a depth of about 50 m in a sedimentary soft mudstone

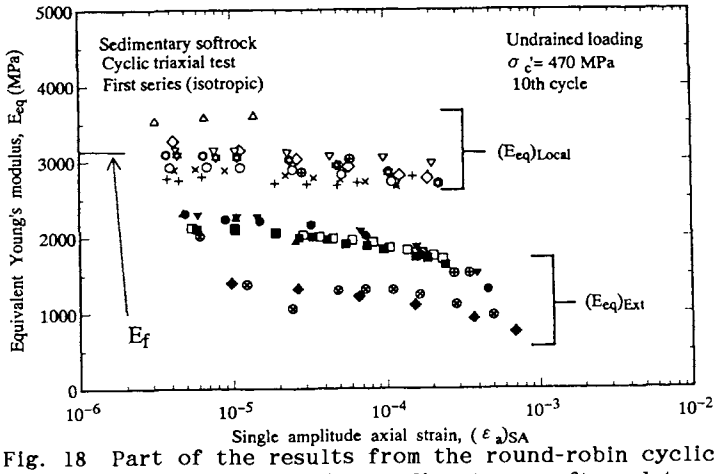

Fig. 18 Part of the results from the round-robin cyclic triaxial test program using sedimentary soft mudstone organized by JSSMFE; comparison of $E_{eq} \sim \log(\varepsilon_a)_{SA}$ relations obtained from eight tests (Fig. 3-16a of Toki et al., 1994).

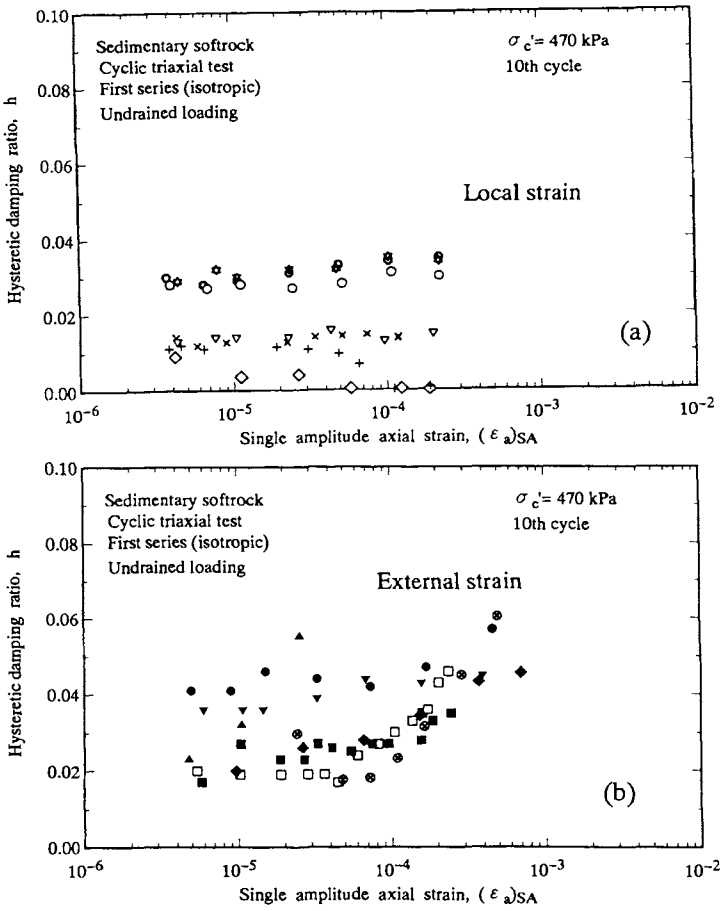

Fig. 19 Part of the results from the round-robin cyclic triaxial test program organized by JSSMFE using sedimentary soft mudstone; comparison of $h \sim \log(\varepsilon_a)_{SA}$ relations, corresponding to Fig. 18; a) local and b) external strain measurements (Fig. 3-17 of Toki et al., 1994).

deposit in Sagamihara City. The geological and geotechnical description of the site is given by Ochi et al. (1993, 1994), Kim et al. (1994), Tatsuoka and Kohata (1995) and Tatsuoka et al. (1995). The compressive strength of the similar samples obtained by CU triaxial compression tests was about 6.8 MPa.

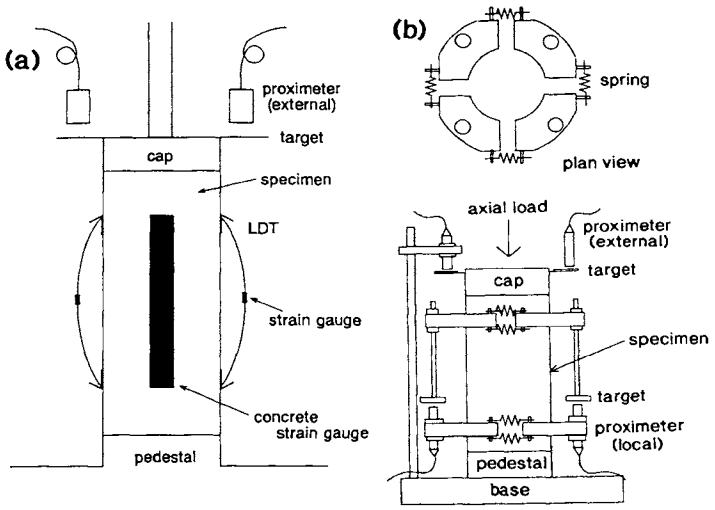

Fig. 20 Three different methods of local axial strain measurement used in the round robin tests on sedimentary soft rock.

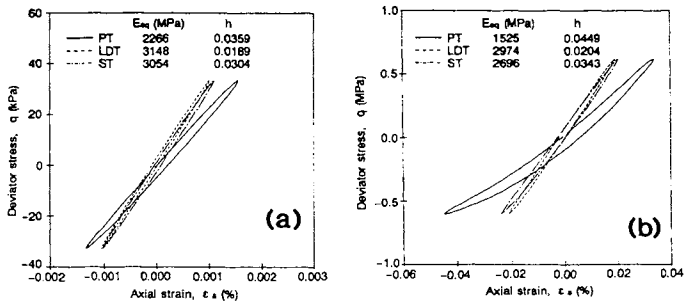

Fig. 21 Stress-strain relations at two loading states from cyclic undrained triaxial loading tests on sedimentary soft mudstone (n.b., PT; external strains measured with a pair of proximeters, and LDT and ST; local strains measured with a pair of LDT and a pair of e.r.s.gs., respectively).

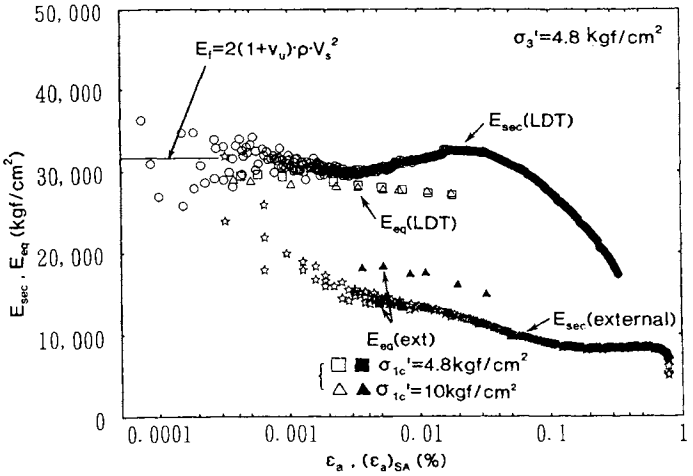

Fig. 22 Comparison of $E_{eq} \sim \log(\varepsilon_a)_{SA}$ relations from a undrained cyclic loading triaxial test with $E_{sec} \sim \log \varepsilon_a$ relations from a CU triaxial compresslon test, using a single specimen of sedimentary soft mudstone from Sagamihara site (Tatsuoka and Kohata, 1995).

After having been water-saturated, the specimens were isotropically consolidated to the field effective over-burden pressure (0.47 MPa). A summary of the data of in total eight tests is shown in **Figs. 18** and **19**. The treatment method of the specimen ends were slightly different for the tests. In six tests, the ends were capped with gypsum, while no capping was carried out in the other two tests. In six tests, at the top and bottom of each specimens, a sheet of filter paper was placed, while in the other two tests, a sheet of Teflon was used. The cyclic loading test procedure was fundamentally the same with that for Toyoura sand, except that cyclic loading tests were performed only under undrained conditions while allowing drainage between two successive cyclic loading stages with different cyclic stress amplitudes (n.b., for Toyoura sand, both drained and undrained cyclic loading tests were performed). The loading frequency f ranged from 0.05 Hz to 1.0 Hz, but the effects of the different frequencies can be ignored as shown later.

The following trends of behavior can be noted from Fig. 18:
1) The E_{eq} values based on locally measured strains are very similar to each other, despite the fact that three different local gages were used (**Fig. 20**). These are a pair of LDTs (Fig. 1b), a pair of electrical resistant strain gages (e.r.s.gs.) with a relatively long gage length (7.0 cm) which was originally for concrete specimens, and a pair of proximeters (PT). For th use of e.r.s.gs., a special measure was taken for the water-tightness. In one laboratory, the local measurements using LDTs and e.r.s.gs. (ST) together with the external measurement with proximeters (PT) were carried out in a single test (**Fig. 21**). It is seen that the stress-strain relations from the two local strain measurements are very similar. It should also be noted that these E_{eq} values based on locally measured axial strains are very similar to the elastic Young's modulus $E_T = 2(1 + \nu_{undrained}) \cdot \rho \cdot V_s^2$ obtained from the field shear wave velocity V_s (Kim et al., 1994, Ochi et al., 1994, Tatsuoka and Kohata, 1995).
2) The E_{eq} values based on externally measured axial strains scatter largely, and they are substantially lower than those based on locally measured axial strains. For all of the test specimens, the range of the consolidated dry density was 1.536 - 1.682 g/cm^3, but the effects of these variations cannot explain the large variations in the data. The difference in the results between the external and local axial strain measurements can be noted also from Fig. 21 (n.b., PT stands for axial strains obtained from the axial displacement of the specimen cap measured with proximeters). This difference is in fact due to the effects of the bedding error.

Fig. 22 compares the $E_{eq} \sim \log(\varepsilon_a)_{SA}$ relations based on externally and locally strain measurements obtained from one of the undrained cyclic loading triaxial test (n.b., the comparison with $E_{sec} \sim \log \varepsilon_a$ relations obtained from a CU triaxial compression test which was performed after cyclic loading is later discussed). This data is included in Fig. 18. In this test, after a series of cyclic undrained loading was performed on an isotropically consolidated specimen, the axial stress was increased to 0.98 MPa under drained conditions, and another series of cyclic loading tests were then performed. It can be seen from Fig. 22 that the effects of different consolidation axial stresses on the E_{eq} value are negligible, while the effects of the bedding error on the E_{eq} values are considerable.

The following trends of behaviour can be noted from Fig. 19;
1) The scatter of the values of h, even based on locally measured axial strains, is large. The reason(s) is(are) not yet known: presumably imperfect confirmation of simultaneous recording of axial stress and strains for some

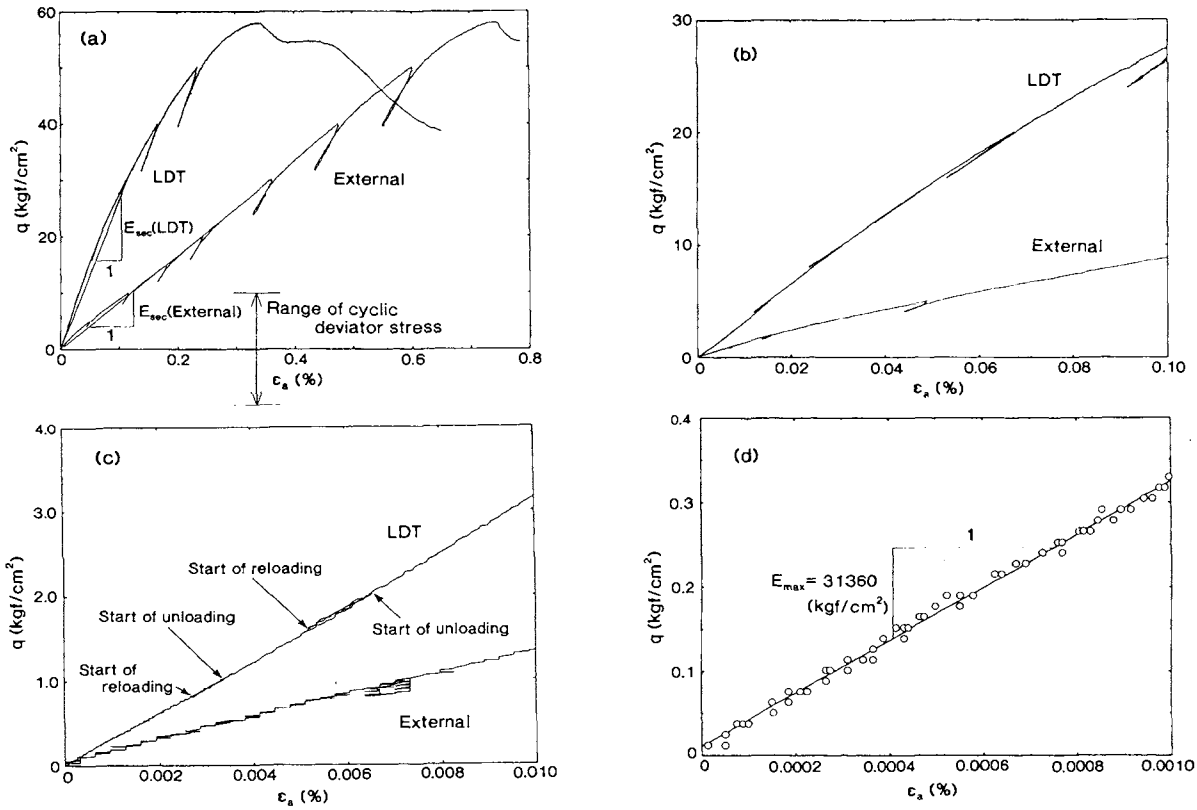

Fig. 23 Stress-strain relation for a wide range of strain from a CU triaxial compression test on undisturbed sample of sedimentary soft mudstone performed after a series of cyclic loading tests; see Fig. 22 (Kohata et al., 1994b).

of the tests may be one of the reasons.

2) The values of h based on externally measured axial strains scatter more largely and these values are larger than the values of h based on locally measured axial strains. The effects of the bedding error should be the major reason for this, since for the same test, the stress-strain relations based on locally measured axial strains have a smaller hysteresis loop area than that based on externally measured axial strains (Fig. 21). The values of h corresponding to the data shown in Fig. 21 are those designated by the symbols ▽(LDT) and ▼(PT) in Fig. 19.

Fig. 23 shows the stress-strain relation for a wide range of strain obtained from a CU triaxial compression test performed on an isotropically consolidated undisturbed sample of sedimentary soft mudstone (σ_c'= 0.47 MPa). This test was performed after a series of cyclic loading tests. The $E_{eq} \sim \log(\varepsilon_a)_{SA}$ relations obtained from the cyclic test are presented in Fig. 22. Very large effects of the bedding error can be noted also in this ML test result.

It is obvious from the above that proper local axial strain measurement is imperative in both ML and cyclic loading (CL) triaxial tests on sedimentary soft rock. The mechanism of the bedding error in triaxial tests on sedimentary soft rock is discussed in more detail by Kim et al. (1994), Tatsuoka and Shibuya (1992) and Tatsuoka and Kohata (1995). One of the major factors for the bedding error is the extra compression of a thin disturbed zone at the top and bottom ends of a specimen, which is inevitably formed by trimming. The other factors are the extra compression of a drainage layer (i.e., filter paper) when used, and the imperfect contact between the specimen ends and the cap and pedestal. The effects of these three factors could not be ignored even after consolidation due to a high rigidity of sedimentary soft rock (Kim et al., 1994).

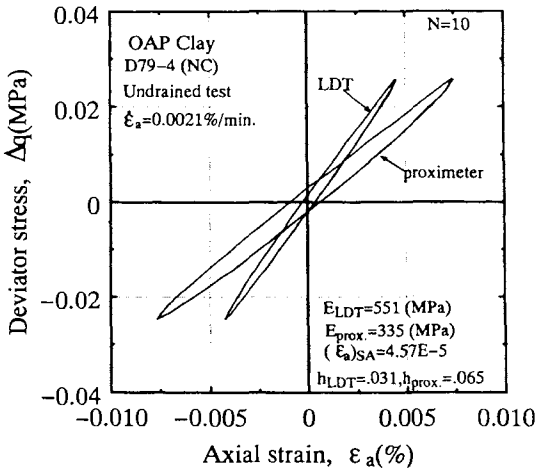

Fig. 24 Typical stress-strain relation from one undrained cyclic triaxial loading on undisturbed OAP clay (tested by Mr. Mukabi,J.N., 1994).

Test results for stiff clay: **Fig. 24** shows typical stress-strain relations obtained from one undrained cyclic triaxial loadings on undisturbed Pleistocene clay (OAP clay)(Mukabi, 1994). The sample was retrieved by thin wall sampling from a depth of 79 m in Osaka City. The specimen (5 cm in D and 12.5 cm in H) was anisotropically consolidated at a nearly constant strain rate of 0.001%/minute to the field effective stress state (σ_v'= 0.674 MPa and σ_h'= 0.337 MPa; n.b., K_o= 0.5 was assumed). In the test, the axial strain was measured both locally using a pair of LDTs (Fig. 1b) and externally from the axial displacement of the specimen cap with a proximeter. The details of the cyclic loading tests are explained in the following section. Very large effects of the bedding

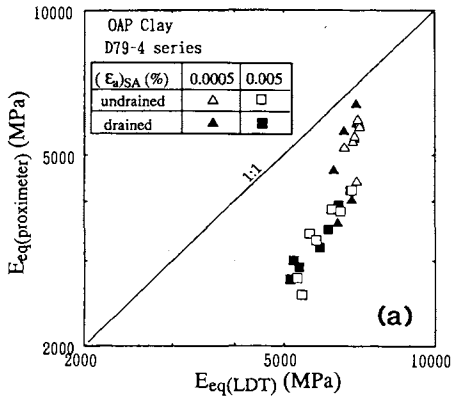

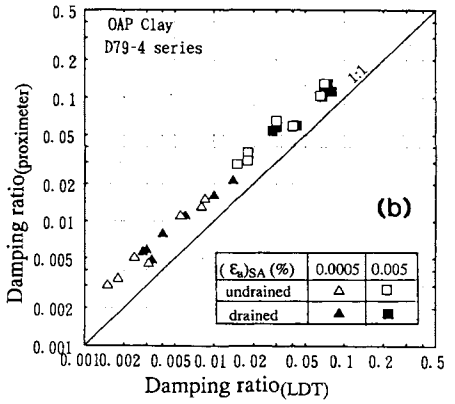

Fig. 25 Comparison of a) E_{eq} values and b) h values based on locally and externally measured axial strains from a series of drained and undrained cyclic triaxial loading on undisturbed OAP clay (tested by Mr. Mukabi,J.N., 1994).

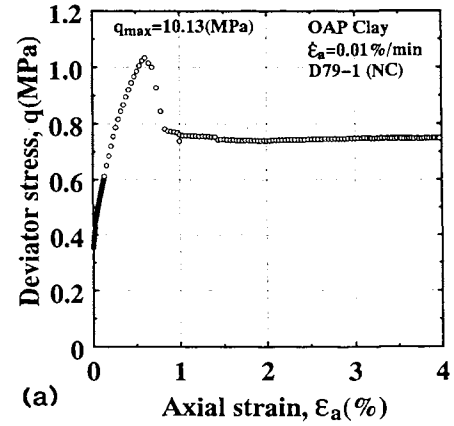

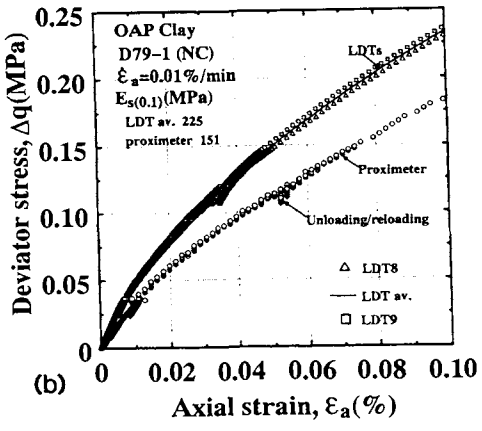

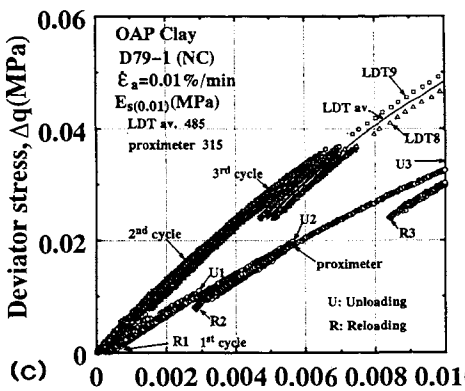

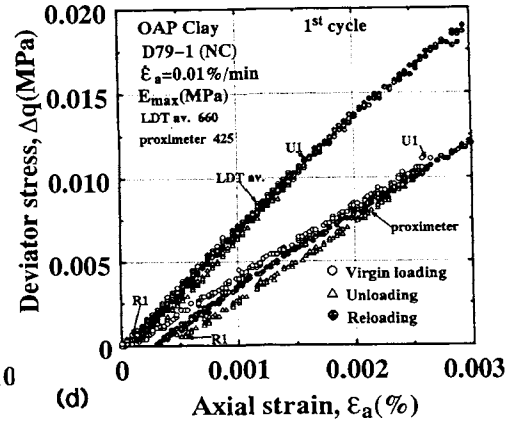

Fig. 26 Stress-strain relations for a wide range of strain from a CU triaxial compression test on undisturbed sample of Pleistocene clay (OAP clay) (tested by Mr. Mukabi,J.N., 1994).

error can be seen. **Figs. 25(a)** and **(b)** compare the values of E_{eq} and h based on locally and externally measured axial strains which were obtained from a series of drained and undrained cyclic triaxial loading cycles on undisturbed OAP clay (tested by Mr. Mukabi, J.N., 1994). Further more, the result of a CU triaxial compression test on Pleistocene clay (OAP) consolidated in the same way with the specimen for cyclic tests described above is shown in **Figs. 26** and **27**. Axial stains were measured also locally and externally (Fig. 20a). In Figs. 26(b) and (c), readings of each of the two LDTs and their average are presented, while in Fig. 26(d), only the average is shown. Large bedding error effects can be seen in these ML and CL test results. Tatsuoka and Kohata (1995) reports the results of other CU triaxial compression tests on OAP clay, which also show large effects of the bedding error. At Politecnico di Torino, a series of CD triaxial tests were performed on undisturbed samples of Pisa clay (PI= 47 - 55) isotropically and anisotropically (K= 0.65) re-consolidated to σ_v (in-situ) = 112 kPa. The samples were retrieved from a depth of 13 m. The compressive strength was about 140 kPa. It was found that the effect of the bedding error on axial strains was noticeable, which was 7 ~ 15 % on average.

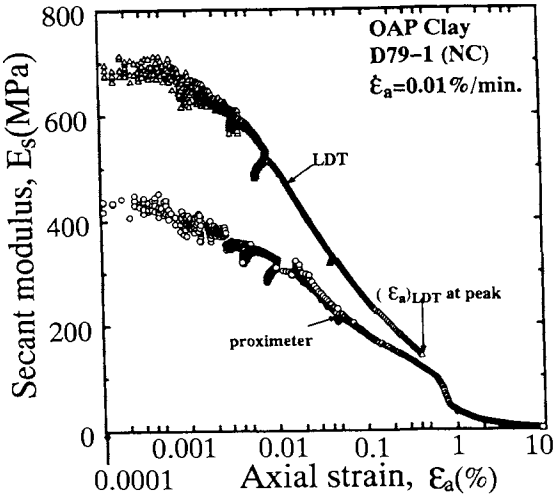

Fig. 27 E_{sec} and ε_a relations for a wide range of strain from a CU triaxial compression test on undisturbed sample of Pleistocene clay (OAP clay), see Fig.26 (tested by Mr. Mukabi,J.N., 1994).

It can be seen from the above that the local strain measurement is imperative also in both ML and CL triaxial tests for stiff clay.

Some other remarks for bedding error: A large amount of data that shows large effects of the bedding error on the axial strains for a wide range of geomaterials is presented in Tatsuoka and Shibuya (1992), Shibuya et al. (1993) and Tatsuoka and Kohata (1995). These are for undisturbed stiff clays of the Pleistocene Era retrieved by thin-wall tube sampling, undisturbed sands of the Holocene Era and Pleistocene Era retrieved by the in-situ freezing method, a volcanic ash clay retrieved by block sampling,

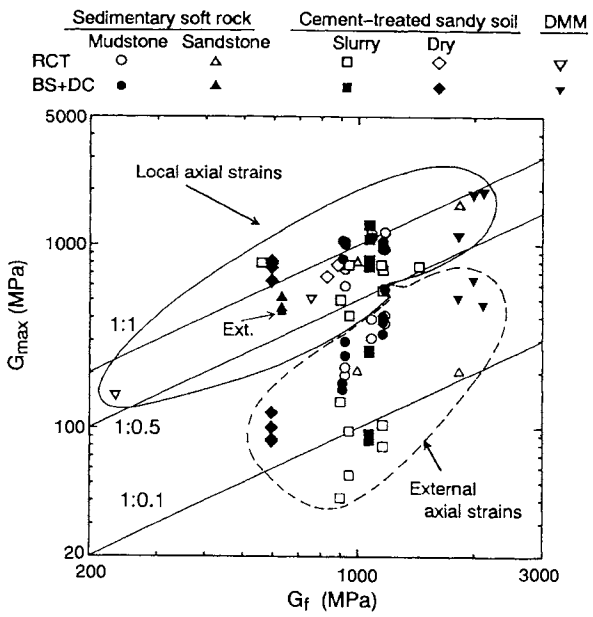

Fig. 28 Comparison between maximum shear modulus G_{max} defined at strains of less than 0.001 % from triaxial tests on undisturbed samples and elastic shear modulus G_T from field shear wave velocity for sedimentary soft rocks and cement-mixed soils (Tatsuoka et al., 1995).

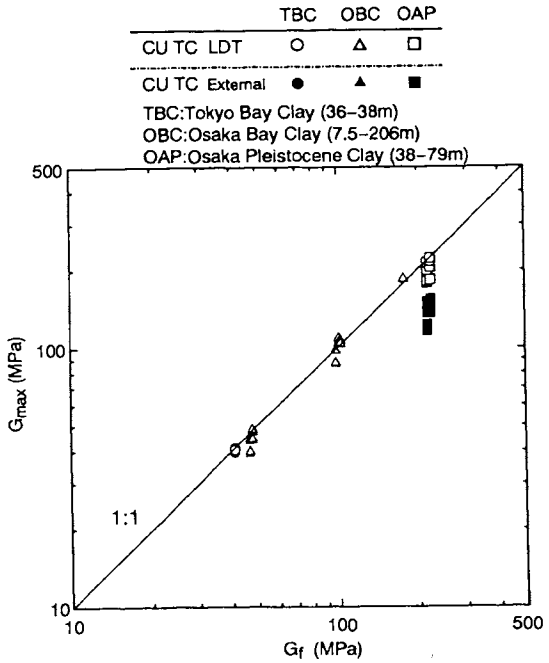

Fig. 29 Comparison between maximum shear modulus G_{max} defined at strains of less than 0.001 % obtained from CU triaxial compression tests on undisturbed samples and elastic shear modulus G_T from field shear wave velocity for Pleistocene clays (Mukabi, 1994, Tatsuoka and Kohata, 1995).

sedimentary soft sandstone and mudstone and cement-mixed sand and clay retrieved by rotary core sampling and block sampling, and cement-mixed cinder compacted in the laboratory. In the authors' laboratories, except when testing on soft clay specimens which exhibit axial strains larger than about 1 % during consolidation, the use of a local gage (e.g., LDTs or LVDTs) is the standard triaxial test procedure.

Our view on sample disturbance could be distorted and biased if based on externally measured axial strains as shown below. **Fig. 28**, which refers to sedimentary soft rock and cement-mixed soil, compares the maximum shear modulus G_{max}, defined at strains of less than 0.001 % obtained from a large number of triaxial tests (mostly CU triaxial compression tests with some cyclic triaxial tests), with the corresponding elastic shear modulus G_T obtained from field shear wave velocity measured at a depth from which the concerned undisturbed samples for the triaxial tests were retrieved (Tatsuoka et al., 1995). Each data point was obtained by averaging several pieces of data obtained under a similar condition. In these triaxial tests, both local and external axial strains were measured. It can be seen from Fig. 28 that all of the laboratory shear moduli G_{max} obtained based on externally measured axial strain are much smaller than each corresponding elastic shear modulus G_T obtained from field shear wave velocities. When based on solely these test results, one may naturally presume that this difference is primarily due to large effects of sample disturbance.

On the other hand, in Fig. 28, the values of G_{max} based on locally measured axial strains are much more similar to the G_T values, in particular for the data of undisturbed samples obtained by block sampling (BS) and direct coring (DC) from the ground surface exposed by excavation. The fact that some data of G_{max} based on local strains for the samples obtained by rotary core tube sampling are noticeably smaller than each corresponding G_T value is due to the effect of sample disturbance, as discussed by Tatsuoka et al. (1995).

Similar to the above, **Fig. 29** compares the maximum shear moduli G_{max} obtained from CU triaxial compression tests with each corresponding elastic shear modulus G_f (the CU triaxial compression tests were performed by Mr. J.N. Mukabi). The samples were obtained by thin-wall tube sampling from deposits of the Pleistocene Era. The specimens were re-consolidated anisotropically with a stress ratio σ'_r/σ'_a (K)= 0.5 to the in-situ pressure level. Each maximum shear modulus G_{max} was defined for the initial part of the stress-strain curve at strains of less than about 0.001 %, which is known to be identical to the G_{eq} value at very small strains obtained from the corresponding cyclic triaxial test as described above. It can be seen that the effect of the bedding error tends to increase as the G_f increases. It can also be seen that on average, the values of G_{max} based on locally measured strains are very close to the G_f values, which indicates a negligible degree of sample disturbance. When based on externally measured axial strains, however, one may consider that the stiffer clay samples have been more disturbed.

The effects of the bedding error on the cyclic undrained strength defined in terms of cyclic stress amplitude (i.e., the so-called liquefaction strength) of saturated uncemented soils obtained from cyclic undrained triaxial tests are usually negligible. For cemented soils, however, it is not always the case as shown below. The flat part of a huge man-made island, Kisarazu Island, of the Trans-Tokyo Bay Highway was constructed by using a kind of cement-mixed sand with a natural water content of about 10 % (Uchida et al., 1993). This material, called the dry type cement-mixed sand, was first prepared in a plant

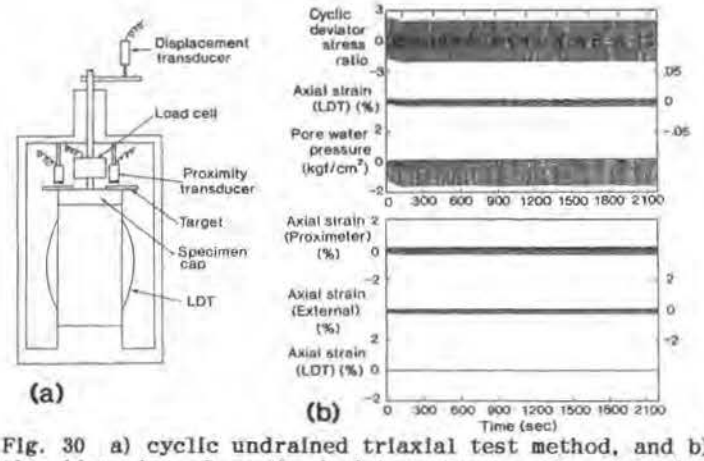

Fig. 30 a) cyclic undrained triaxial test method, and b) time histories of cyclic deviator stress ratio, excessive pore water pressure and axial strains from a typical cyclic undrained triaxial test on cement-mixed sand used for Trans-Tokyo Bay Highway Project.

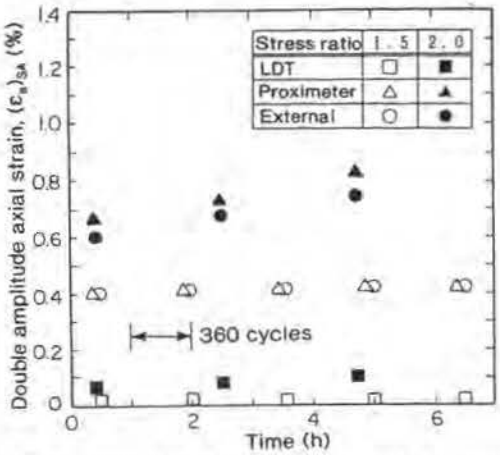

Fig. 31 Time histories of double amplitude axial strain from two cyclic undrained triaxial tests of cement-mixed sand used for Trans-Tokyo Bay Highway Project.

vessel at sea, and was then poured into the sea from the sea surface by means of a specially designed devise. The total volume of the material used was 435,000 m^3. At the design stage prior to the construction, it was considered that the shear strength of the material after having been placed under water would not be very large. In fact, the CU triaxial compression tests on core samples obtained by rotary core tube sampling performed 120 - 290 days after the construction showed a compressive strength ranging from 0.63 to 1.0 MPa. The seismic stability of the fill during major earthquakes was, therefore, one of the major concerns in the design.

A series of cyclic undrained triaxial tests were performed using samples of 7.5 cm in D and 15 cm in H obtained by block sampling from a fill constructed under water in a trial placement test. The compressive strength obtained from CU triaxial compression tests with σ_c' = 49 kPa was about 0.8 MPa. For the cyclic undrained triaxial tests, each specimen was first saturated so that the B value was 0.95 or more, and was then isotropically consolidated to σ_c' = 49 kPa. In the cyclic tests, axial strains were measured by three methods as shown in **Fig. 30(a)**. **Fig. 30(b)** shows the time histories of the cyclic deviator stress ratio SR= $(\sigma_a-\sigma_r)/(2\sigma_c')$, the excessive pore water pressure and the axial strains obtained from a typical cyclic undrained triaxial test on the cement-mixed sand performed at a loading frequency of 0.1 Hz. The single amplitude of $(\sigma_a-\sigma_r)/(2\sigma_c')$, denoted by SR, was as large as 2.0. It can be seen that, despite the large cyclic stresses applied, the single amplitude of locally measured axial strain remained at a very small value, about 0.1 %, and did not exhibit a tendency to increase with cyclic loading. **Fig. 31** summarizes the time histories of double amplitude axial strains obtained from two other cyclic undrained triaxial tests with SR= 1.5 and 2.0, in which cyclic undrained loading was continued for more than six hours. Again, the locally measured axial strain was very small, and based on this result, it was judged that noticeable cyclic strain-softening of this material during design earthquake loading would be unlikely. On the other hand, it may be seen from Figs. 30 and 31 that the externally measured axial strains were much larger than those locally measured, which is, however, a totally misleading result.

ELASTIC DEFORMATION CHARACTERISTICS OF GEOMATERIALS

Elasticity: The elastic deformation properties are characterized by both 1) recoverable deformation and 2) strain rate-independent stress-strain relationships. For a wide range of geomaterials, the deformation properties are essentially elastic for a range of strain less than about 0.001 %. For this strain range, no major slipping occurs at interparticle contact in uncemented soils and no major micro-cracks are produced in cemented soils and rocks. It is considered that plastic deformation is associated with the above mentioned permanent changes or destruction of the inherent structure, and is therefore strain rate-dependent.

Fig. 32 shows the stress-strain relation obtained from a CD triaxial compression test on an undisturbed sample of sedimentary soft silty-sand-stone (D_{50}= 0.072 mm). The sample, 5.0 cm in D and 15 cm in H, was obtained by rotary core tube sampling at a depth of 23 m at Kan-nonzaki site as part of a geotechnical investigation for a giant suspension bridge at the entrance to the Tokyo Bay under consideration, which will be even longer than the world's longest suspension bridge (Akashi Strait Bridge). The specimen was re-consolidated isotropically to the field effective over-burden pressure σ_v'(in-situ)= 0.265 MPa. Several small unload/reload cycles were applied during otherwise monotonic loading. Large effects of the bedding error may be noted. It can be seen that the behaviour at axial strains less than about 0.01 % is nearly linear and recoverable, see also Fig. 23. A test result of a CU triaxial compression test on Pleistocene clay (OAP), similar to the above, is shown in Fig. 26.

The extent of elastic properties and the manner of their change with shear straining can be most conveniently examined by this type of monotonic loading test shown in Figs. 26 and 32, as discussed in detail by Tatsuoka et al. (1994b). This testing method has been used also in rock mechanics and concrete engineering to investigate the damage to the material structure based on the change of elastic modulus. A great deal of similar data is shown in Tatsuoka and Shibuya (1992) and Tatsuoka and Kohata (1995).

Static monotonic and cyclic tests versus dynamic tests: When the deformation is elastic, the same elastic stiffness should be obtained from dynamic and static (monotonic and

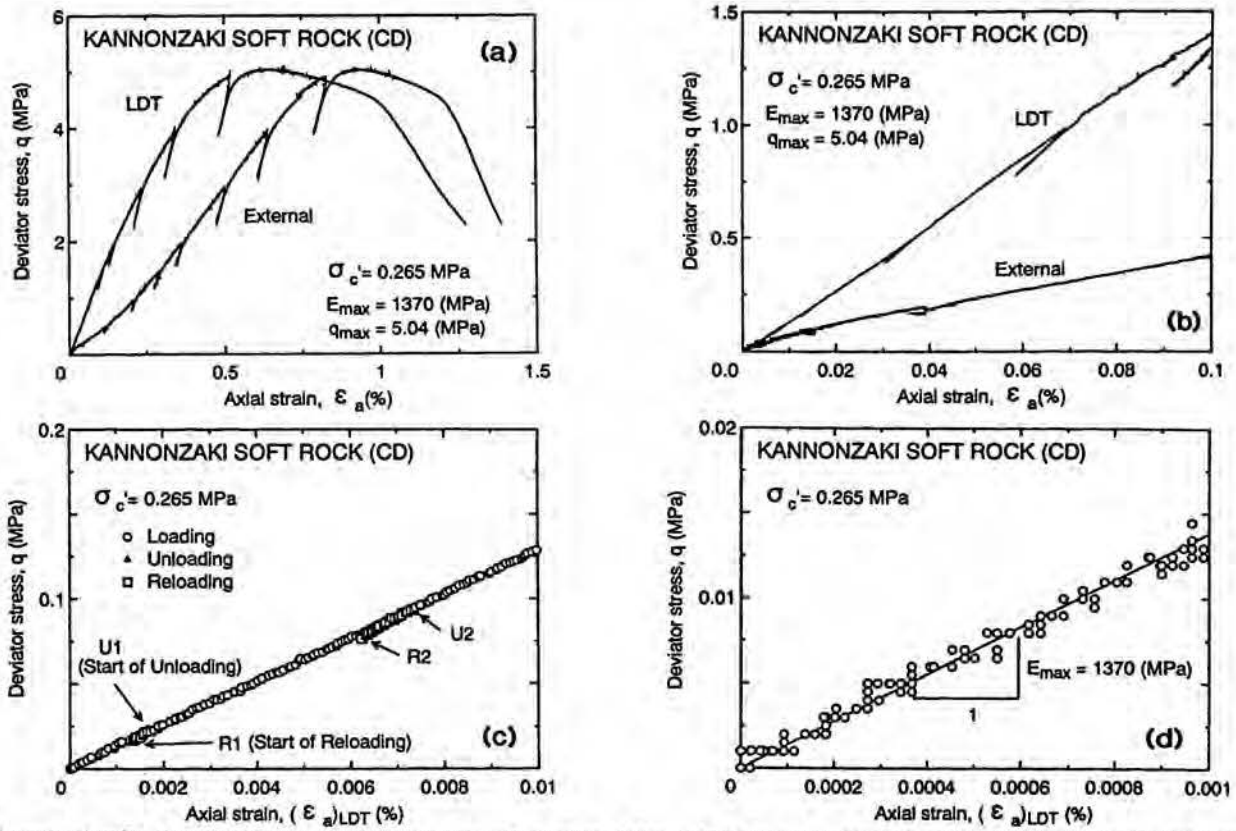

Fig. 32 Stress-strain relation for a wide range of strain from a CD triaxial compression test on undisturbed sample of sedimentary soft silty-sand-stone from Kan-nonzaki site.

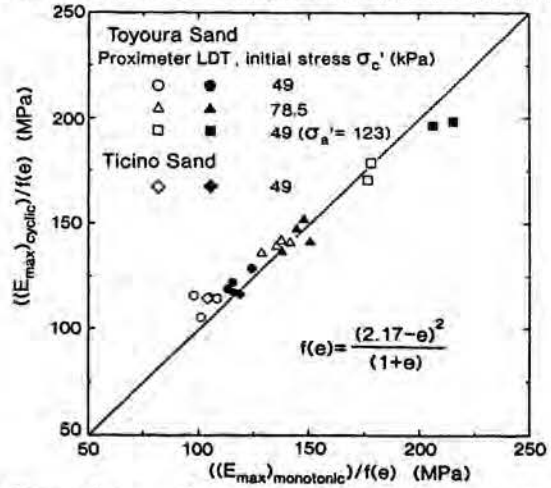

Fig. 33 Comparison of E_{max} values from triaxial compression tests and cyclic triaxial tests for air-pluviated Toyoura sand (Tatsuoka et al., 1994a).

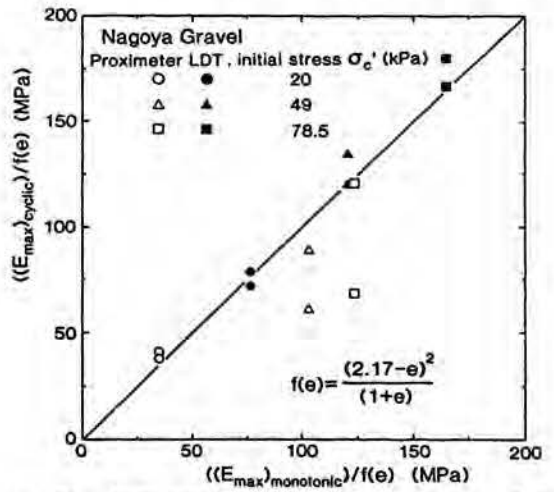

Fig. 34 Comparison of E_{max} values from triaxial compression tests and cyclic triaxial tests for Nagoya gravel (Dong et al., 1994, Kohata et al., 1993).

cyclic) loading tests performed under otherwise the same testing conditions as shown below.

In Fig. 6d for a ML triaxial compression test on loose Toyoura sand, the initial Young's modulus E_{max} is defined at axial strains less than 0.001 %. The E_{max} value from this test and similar other tests are compared with those determined from the corresponding cyclic triaxial tests performed under otherwise the same testing conditions in **Fig. 33**. In this figure, the E_{max} values have been normalized by the void ratio function $F(e)= (2.17 - e)^2/(1 + e)$ to eliminate the effects of the variations in void ratio. It can be seen that each pair of Young's moduli, determined by monotonic and cyclic loading tests, are almost the same. In this case, the E_{max} values based on either locally or externally determined axial strains are similar between ML and CL tests, although the E_{max} values are different due to the bedding error effects.

A very good agreement of the E_{max} values obtained from a pair of ML and CL triaxial tests can be also seen in Figs. 4 and 5 for Toyoura sand, Fig. 15a for Nagoya gravel and Fig. 22 for sedimentary soft mudstone. **Fig. 34** shows a comparison for Nagoya gravel, similar to Fig. 33. In this case, the E_{max} values obtained from ML and CL tests are very similar only when based on locally measured axial

Table 3 E_{max} values of Toyoura sand obtained from a series of CD triaxial compression tests on isotropically and anisotropically consolidated specimens performed in Torino (Lo Presti et al., 1995, Pallara, 1995).

σ'_v [kPa]	σ'_h [kPa]	K	Stress history	e	E_{max} [MPa]	$E_{max}/F(e)$ [MPa]	$E_{max}\times F(e=0.69)/F(e)$ [MPa]
102.2	46.1	K_o=0.46	NC	0.799	240	230	298
100.8	69.6	0.69	NC	0.785	240	223	289
101.4	100.5	0.99	NC	0.782	225	208	270
97.2	150.5	1.55	NC	0.790	220	207	268
98.9	201.4	2.04	NC	0.766	250	224	290
99.7	67.1	K_o=0.67	OCR=3	0.776	255	233	302
99.0	98.9	1.00	R_o=3	0.789	230	216	280
100.8	46.4	0.46	R_o=3	0.778	220	202	262

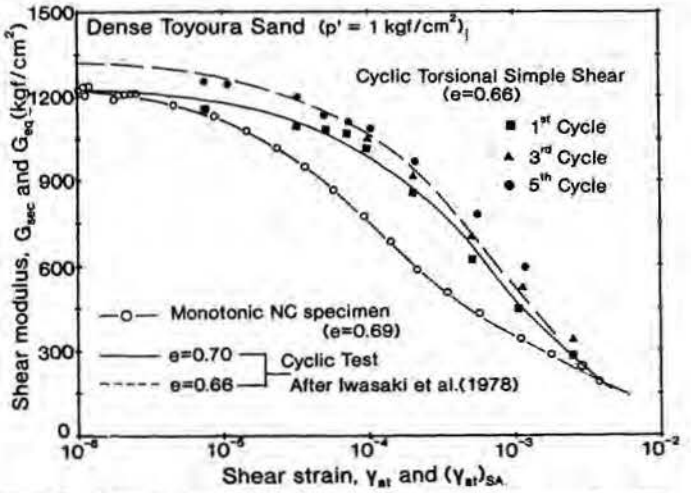

Fig. 35 Comparison of shear modulus and shear strain relations of Toyoura sand from monotonic and cyclic torsional shear tests and torsional resonant-column tests (Teachavorasinskun et al., 1991).

strains, but it is not the case when based on externally measured axial strains. This is due to different amounts of the effects in the ML and CL triaxial tests. It is to be noted that the E_{max} values of Toyoura sand which are almost the same with those obtained from the round robin tests have been obtained from a series of CD triaxial compression tests on isotropically and anisotropically consolidated specimens which were performed independently in Politecnico di Torino (**Table 3**). In these tests, the axial strains were measured locally by means of LVDTs or LDTs. This agreement also indicates that we can obtain fundamentally the same elastic stiffness from ML and CL tests.

Fig. 35 compares the shear moduli of Toyoura sand obtained from ML and CL torsional shear tests using hollow cylindrical specimens (10 cm and 6 cm in outer and inner diameters and 20 cm high). The shear strain rate was 0.01 %/min. It can be seen that at strains of less than 0.001 %, the stiffness is very similar between the two types of tests. Two continuous curves, solid and broken ones, were obtained by a series of torsional resonant-column tests (for shear strains ≤ 0.04 %) and cyclic torsional shear tests (for shear strains ≥ 0.003 %) (Iwasaki et al., 1978).

Fig. 36 summarizes the shear moduli of Toyoura sand obtained from triaxial compression tests (TXTs; Table 3), static ML torsional tests and torsional resonant-column tests which have been obtained independently at IIS, University of Tokyo and Politecnico de Torino. An

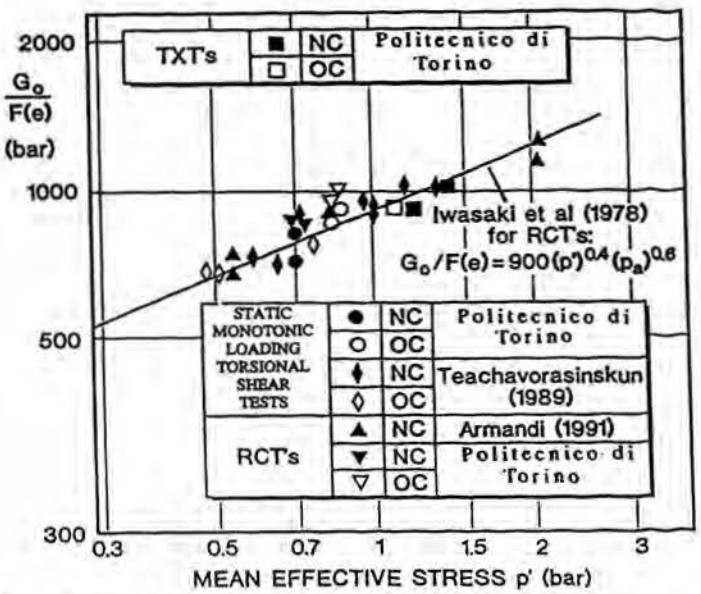

Fig. 36 Comparison of the maximum shear moduli G_{max} plotted against mean pressure p of Toyoura sand obtained from several different testing methods; $F(e)= (2.17- e)^2/(1 + e)$ (Jamiolkowski et al., 1994); For the four static ML torsional shear tests (Jamiolkowski et al., 1994), the specimens were 7.1 cm and 5.0 cm in outer and inner diameters and 14.2 cm high and the void ratios were 0.66, 0.75, 0.87 and 0.9. For the resonant column tests, the specimens were either solid cylinder (four tests with 5.0 cm in D and 10 cm in H; Armandi, 1991) with void ratios of 0.68, 0.71, 0.84 and 0.87 or hollow cylinder (four tests with 5.0 cm in ID, 7.1 cm in OD and 14.2 cm in H) with void ratios of 0.66, 0.75, 0.87 and 0.9.

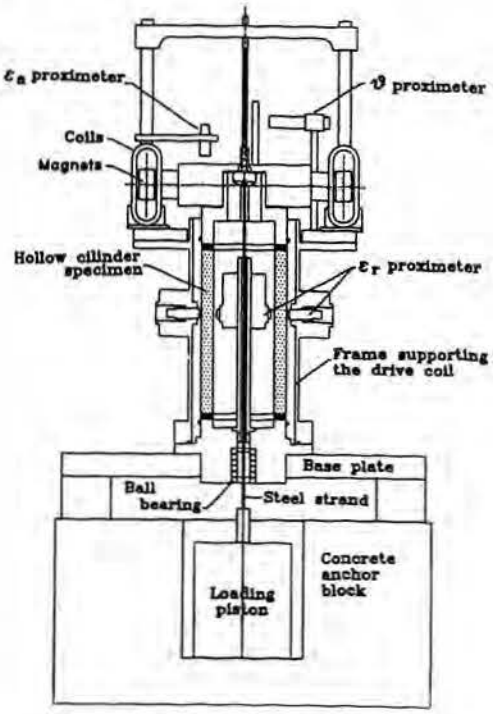

Fig. 37 Resonant-column/torsional shear apparatus using a hollow cylinder specimen (denoted as THCST in Fig. 36) used in Torino (Lo Presti et al., 1993).

empirical relation based on resonant-column test data (Iwasaki et al., 1978) is also shown in Fig. 36. **Fig. 37** shows the torsional shear apparatus which is being used at Politecnico di Torino. The average shear strain rate in the static ML torsional shear tests was 0.001%/min. The shear strain rate in the resonant-column tests were 10 - 500 %/min. (also in the tests on Ticino and Quiou sand shown below). A very good agreement can be seen among these data in spite of the different testing methods, particularly between the static and dynamic tests, and different laboratories. A noticeable difference between NC and OC specimens cannot be seen either. This conclusion has also be obtained by Teachavorasinskun et al. (1991).

A comparison of the elastic shear moduli G_{max} for Ticino sand, similar to Fig. 35, is shown in **Fig. 38**. In this figure, the results of ML and CL triaxial tests and ML and CL torsional shear tests performed under a constant confining pressure are compared with that obtained from a torsional resonant-column test. It can be seen that the initial shear modulus at strains of less than about 0.001 % is almost the same not only between the ML and CL static tests, but also between the static and dynamic tests. A comparison of the G_{max} values obtained from static (ML and CL) torsional tests (at a shear strain rate of 0.02 - 0.002 %/min.) and torsional resonant-column tests on Ticino sand are shown also in **Figs. 39(a)** and **(b)** (n.b., the test results on cyclically prestrained Ticino sand shown in Fig. 39b will be discussed later). In Figs. 39(a) and (b) an empirical equation for the G_{max} value of Ticino sand based on the resonant-column test results (Lo Presti 1987, Armandi 1991) and two relations for $\pm$ 12 % deviation from this equation, are presented. The other relation presented for the full range of void ratio in Fig. 39(b) represents the empirical relation proposed for cohesionless soils (Jamiolkowski, et al., 1991). The results of Quiou sand is also shown in Fig. 39(b), which were obtained from torsional resonant-column tests and static ML torsional shear tests at a shear strain rate of 0.001 %/min. Again a very good agreement between the static and dynamic tests can be seen in the data of Ticino sand shown in Figs. 39(a) and (b). For a carbonate crushable sand (Quiou sand), the G_{max} value is slightly higher in resonant-column tests than in static ML tests, with a difference being about 20 %. It is likely that the difference is, at least partly, due to the effects of many cycles of cyclic loading in resonant-column tests and creep deformations involved even at very small strains in ML tests. A good agreement seen between Ticino sand and Quiou sand seen in Fig. 39(b) should be fortuitous.

A good agreement between the torsional shear tests and the triaxial tests can be seen in Figs. 36 and 38. A similar result for other types of sands are reported in Tatsuoka and Kohata (1995). This agreement is probably due to rather isotropic elastic properties in this case (Park and Tatsuoka, 1994).

These results suggest that even by using monotonic loading tests, the elastic stiffness can de evaluated accurately. One should note that the initial stiffness evaluated at very small strains is the elastic stiffness evaluated at the initial stress state. For uncemented and lightly cemented geomaterials, the elastic stiffness in the axial direction increases as the axial stress increases during monotonic loading (Kohata et al., 1994a, Tatsuoka and Kohata, 1995). Another important point is that the stress-strain relation at relatively small strains during monotonic loading can be estimated based on the elastic stiffness by taking into account non-linearity. This estimation could be more accurate for geomaterials with a larger linear elastic zone such as stiff clays (Fig. 26) and

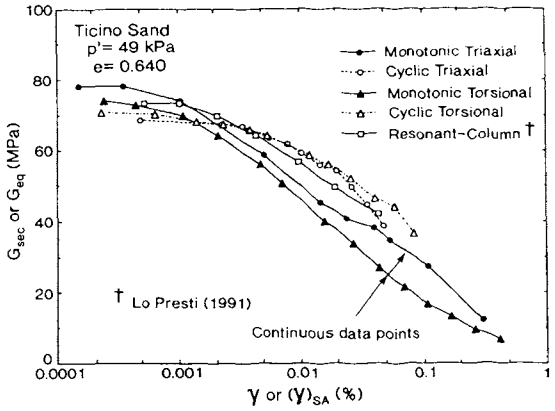

Fig. 38 Comparison of shear modulus and shear strain relations of Ticino sand from a triaxial compression test, a cyclic triaxial test, a pair of monotonic and cyclic torsional shear tests and a torsional resonant-column test; the radial strain was measured locally in the triaxial tests (Teachavorasinskun, 1992, Tatsuoka et al., 1994a, Tatsuoka and Kohata, 1995).

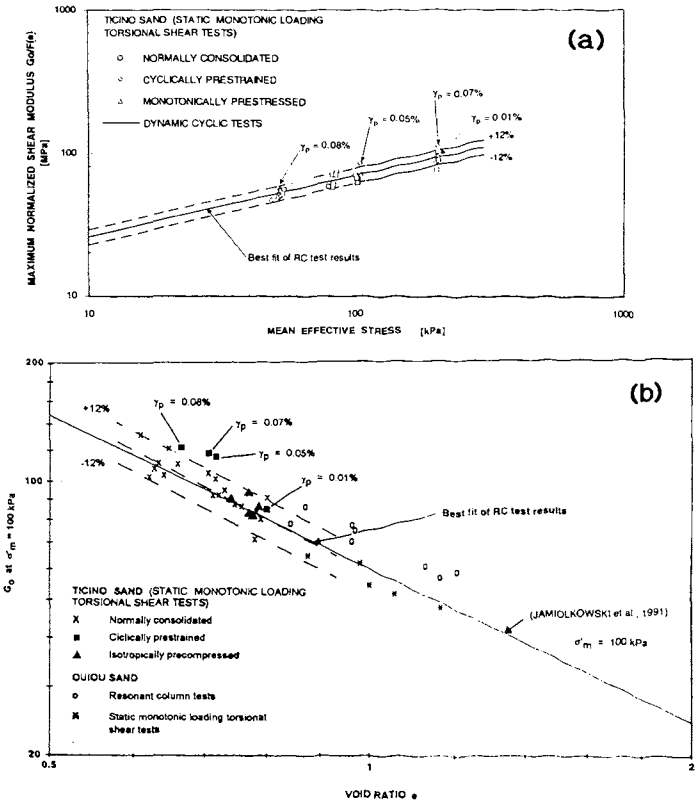

Fig. 39 Comparison of the maximum shear moduli G_{max} plotted against (a) mean pressure p of Ticino sand, and (b) void ratio of Ticino sand and Quiou sand for σ_m= 100 kPa, obtained from several different testing methods (Lo Presti et al., 1993); For the resonant-column tests, the specimens were solid cylindrical (66 tests with 7.1 cm in D and 14 cm in H; Lo Presti, 1987, and four tests with 5 cm in D and 10 cm in H; Armandi, 1991). For 27 static ML torsional shear tests, he specimens were solid cylindrical (5 cm in D and 10 cm in H) at a shear strain rate of 0.002%/min. (Armandi, 1991, Lo Presti et al., 1993). For Quiou sand, the torsional resonant-column tests were five tests with 5 cm in D and 10 cm and three tests with 7.1 cm in OD, 5 cm in ID and 14.2 cm in H), and the static ML torsional shear tests were five tests (7.1 cm in OD, 5 cm in ID and 14.2 cm in H) (Lo Presti et al., 1993, Pallara, 1995).

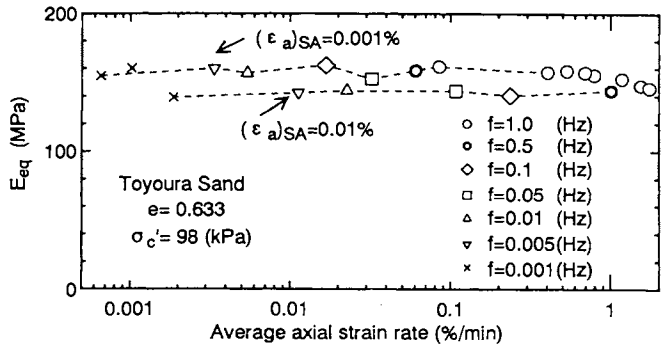

Fig. 40 Effect of strain rate on Young's modulus in drained cyclic triaxial tests on saturated Toyoura sand (Tatsuoka and Kohata, 1995, Kohata et al., 1994b)

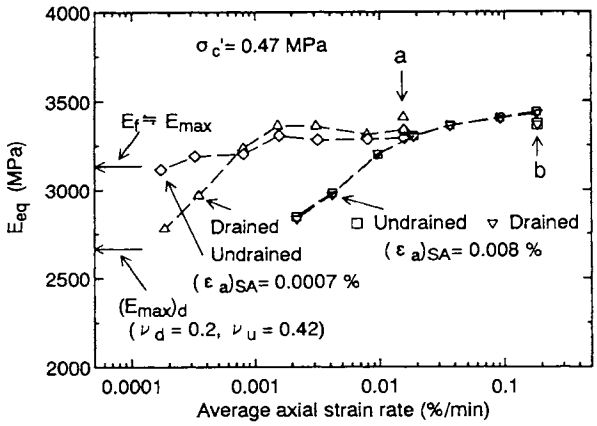

Fig. 41 Effect of strain rate on Young's modulus in drained and undrained cyclic triaxial tests on sedimentary soft mudstone from Sagamihara site (Tatsuoka and Kohata, 1995, Kohata et al., 1994b)

sedimentary softrocks (Figs. 23 and 32). Based on this result, for analysing several case records of geotechnical construction, the non-linear stiffness, which may be either dependent on or independent of pressure level, of the ground was estimated from field shear wave velocities. Full-scale field behaviour such as the settlement of structure foundations and the deformation of deep and large shafts were then successfully explained (Tatsuoka and Kohata, 1995). These topics are again discussed later in this paper.

Strain rate-dependency: The data shown above indicates very small effects of strain rate on the small strain stiffness of sand. More direct and rigorous evaluation of the strain rate effect can be made by performing a test using a single specimen in which the strain rate is varied for a wide range as shown below.

Figs. 40 and **41** show the effects of strain the rate on the Young's modulus E_{eq} obtained from cyclic triaxial tests on Toyoura sand and sedimentary soft mudstone from Sagamihara site, respectively. The test conditions were the same with those for the round robin test programs except for the following points;

(1) The loading frequency of cyclic sinusoidal deviator stresses was changed for a wide range. The peak-to-peak average axial strain rate (%/min) was defined as $240 \cdot f(Hz) \cdot (\varepsilon_a)_{SA}(\%)$. For Toyoura sand, drained cyclic loading was started at a loading frequency f= 1.0 Hz, where measurements of E_{eq} and h were made while increasing the strain amplitude $(\varepsilon_a)_{SA}$. Then, at smaller frequencies, the measurements were made first at $(\varepsilon_a)_{SA}$= about 0.001 % and then at about 0.01 %. For the sedimentary soft rock, a series of cyclic loadings was performed first at $(\varepsilon_a)_{SA}$= 0.0007 % and then at 0.008 %. At each of the strain amplitudes, cyclic loadings were started from the largest strain rate, preceding to those at smaller strain rates, and finally cyclic loadings at the largest strain rate were performed again to see the effect of the previous cyclic loadings.

(2) For sedimentary soft rock, first ten cycles of cyclic deviator stresses were applied under undrained conditions at each cyclic loading stage, and then another ten cycles under "nominally drained" conditions with the drainage valves connected to the top and bottom of the specimen open. The degree of drainage in the "nominally drained" test depends on the strain rate, as discussed below.

At each loading stage with a fixed strain rate and a fixed strain amplitude, ten cycles of cyclic deviator stress was applied. The data at the tenth cycle are presented in Figs. 40 and 41. The following trends may be seen from these figures:

1) For Toyoura sand, the strain rate-dependency of the E_{eq} value is negligible for $(\varepsilon_a)_{SA}$= 0.001 %~0.01 %.

2) For sedimentary soft mudstone, at $(\varepsilon_a)_{SA}$= 0.0007 %, the effect of strain rate on the E_{eq} value is very small under undrained conditions. This point can be noted also from the stress-strain relations shown in **Fig. 42(d)**, in which, for the convenience of comparison, the stress-strain relations have been shifted so that they have a common origin (n.b., the symmetrical cyclic deviator stresses were applied to an isotropically consolidated specimen).

3) For sedimentary soft mudstone, the strain rate effect under the "drained" condition is noticeable even at $(\varepsilon_a)_{SA}$= 0.0007 % at strain rates smaller than 0.001 %/min. (see also **Fig. 42c**). This is due to the fact that as the strain rate decreases, the "drained sample" is better drained and the Young's modulus E_{eq} at small strains under the fully drained condition is smaller than that under the undrained condition by a factor of $(1 + \nu_{drained})/(1 + \nu_{undrained})$, as discussed in detail by Tatsuoka and Kohata (1995). This factor is equal to 0.85 for $\nu_{drained}$= 0.2 and $\nu_{undrained}$= 0.42.

4) For sedimentary soft mudstone, at $(\varepsilon_a)_{SA}$= 0.008 %, the behaviour is almost the same between undrained and "drained" tests, which means that the "drained" tests were actually undrained tests. Their stress-strain relations were, therefore, not discernible (see **Figs. 42 a** and **b**).

5) For sedimentary soft mudstone, at $(\varepsilon_a)_{SA}$= 0.008 %, the strain rate effect is not small. However, the increase in E_{eq} with the increase in the stain rate is upper-bounded by the value of E_{max} observed at $(\varepsilon_a)_{SA}$= 0.0007 %, which is perhaps the true strain rate-independent elastic Young's modulus. As indicated in Fig. 41, this Young's modulus E_{max} is very close to the elastic Young's modulus E_T obtained from the field shear wave velocity at the depth from which the sample was retrieved (Kim et al., 1994; see also Fig. 28).

A result similar to the above was recently obtained from a cyclic triaxial test on a undisturbed sample of Pleistocene clay (OAP clay) (**Fig. 43**). A series of cyclic triaxial loadings were applied at controlled constant but different axial strain rates. At each loading stage with a constant axial strain amplitude and a constant strain rate, ten cycles of cyclic symmetrical axial strains were applied under undrained conditions and then under "nominally drained" conditions. The specimen was allowed to be drained between the undrained and "drained" tests.

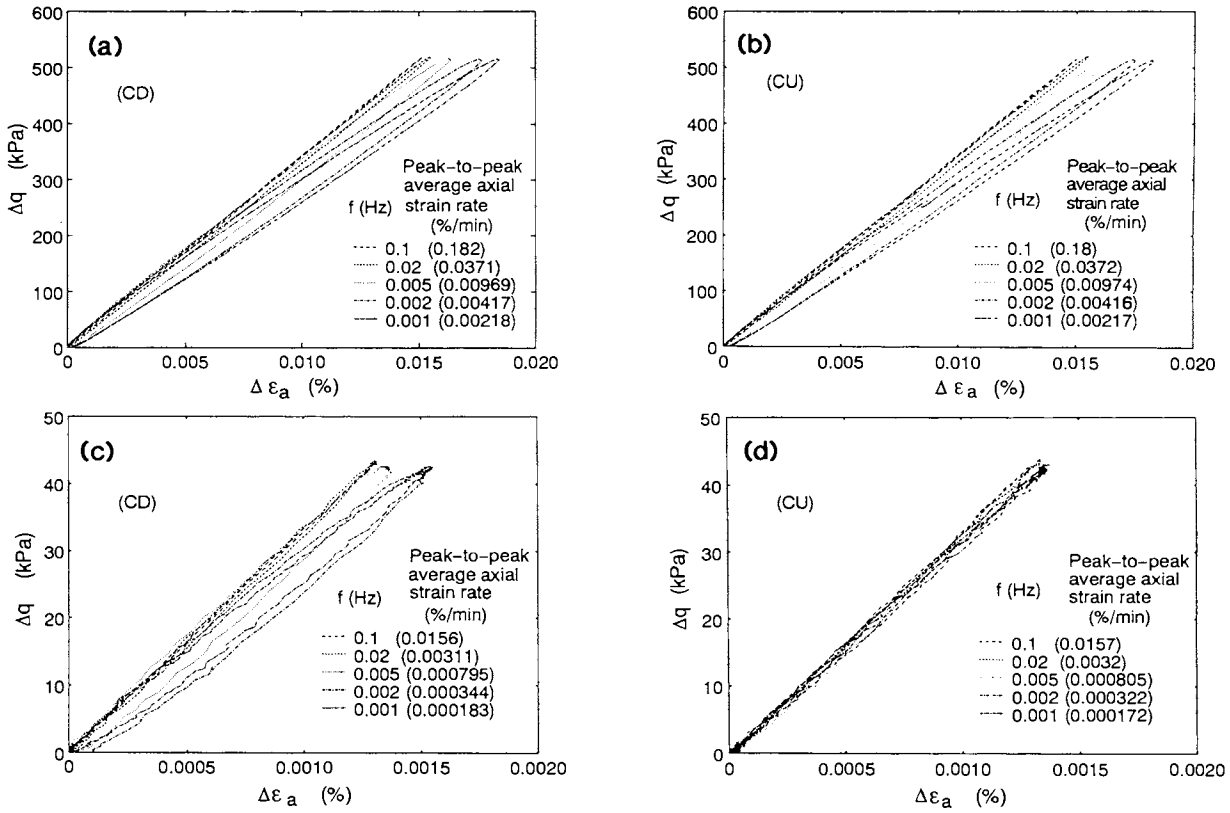

Fig. 42 Stress-strain rations for different strain rates from cyclic triaxial tests, Sagamihara sedimentary soft mudstone; a) (ε_a)$_{SA}$= 0.008 %, "drained", b) (ε_a)$_{SA}$= 0.008 %, undrained, c) (ε_a)$_{SA}$= 0.0007 %, "drained", d) (ε_a)$_{SA}$= 0.0007 %, undrained (Kohata et al., 1994).

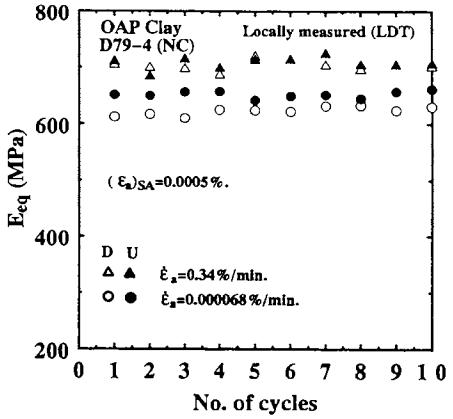

Fig. 43 Effect of cyclic loading on Young's modulus in typical undrained cyclic triaxial tests on saturated Pleistocene clay; OAP clay from Osaka City (tested by Mr. Mukabi,J.N., 1994).

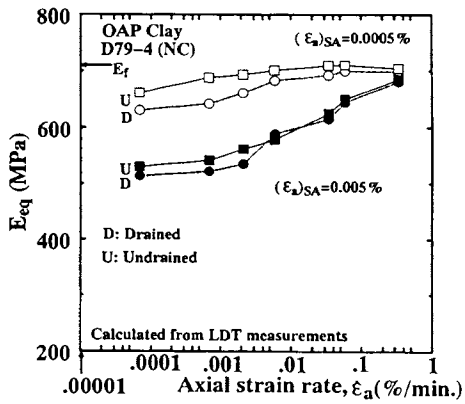

Fig. 44 Effect of strain rate on Young's modulus in drained and undrained cyclic triaxial tests on saturated Pleistocene clay; OAP clay from Osaka City (tested by Mr. Mukabi,J.N., 1994).

The strain rate was decreased first at (ε_a)$_{SA}$= 0.0005 % and then at 0.005 %. Typical stress-strain relations are shown in Fig. 24.

The E_{eq} values based on locally measured axial strains were summarized in **Fig. 44**. It can be seen that the effects of strain rate on the E_{eq} value is very small for (ε_a)$_{SA}$= 0.0005 %, particularly under the undrained condition. On the other hand, the effect becomes noticeable for (ε_a)$_{SA}$= 0.005 %. The difference in the E_{eq} value between the "drained" and undrained tests is noticeable at smaller strain rates when (ε_a)$_{SA}$= 0.0005 %, but the difference becomes less discernible as the strain rate increases.

This feature is also seen for (ε_a)$_{SA}$= 0.005 %, but the effect of drainage conditions is smaller. These features are similar to those observed for sedimentary soft mudstone. It is also important to note that also for this clay, the upper bound undrained Young's modulus E_{max} is very similar to the E_f value obtained from field shear wave velocities as indicated in Fig. 44 (Mukabi et al., 1994) (see also Fig. 29). This value is also very similar to the E_{max} value equal to 647 MPa defined for the initial part of stress-strain relation at axial strains of less than about 0.001 % obtained from a CU triaxial compression test performed at an axial strain rate of 0.01 %/min. (Figs. 26d and 27).

Figs. 45(a) and **(b)** compares shear modulus and shear strain relations for two undisturbed samples of Pisa clay. The relations shown in each figure were obtained from a ML drained torsional shear test at a shear strain rate of about 0.014%/min. and a resonant-column test which was performed subsequently to the ML static test. The specimen was kept undrained throughout the resonant-column test. It can be seen that the shear modulus at very small strains is similar between the static and dynamic tests despite a large difference in the shear strain rate; a slightly larger value by about 15 ~ 20 % obtained by the resonant-column test would be due partly to the strain rate effect and partly to the effect of the previous strains experienced in the static drained test. The difference between the two tests increases noticeably with the increase in the shear strain. This deviation should be principally due to the effect of the strain rate, which increases nearly proportionally with the shear strain in the resonant-column test; the shear strain rate in the resonant-column test increased with the increase in shear strain from about 15 to 1900 %/min. The agreement in the shear modulus between the static ML test and the resonant-column test seen again at large strains exceeding about 0.5 % would be due to a reduction in the shear modulus caused by an increase in the pore water pressure in the resonant-column test.

Summarizing the test results descried above, it can be concluded that the deformation characteristics at strains of less than about 0.001 % of a wide range of geomaterials are nearly recoverable and strain-rate independent, namely elastic. Therefore, very similar elastic stiffness should be obtained from different laboratory and field test performed under otherwise similar conditions.

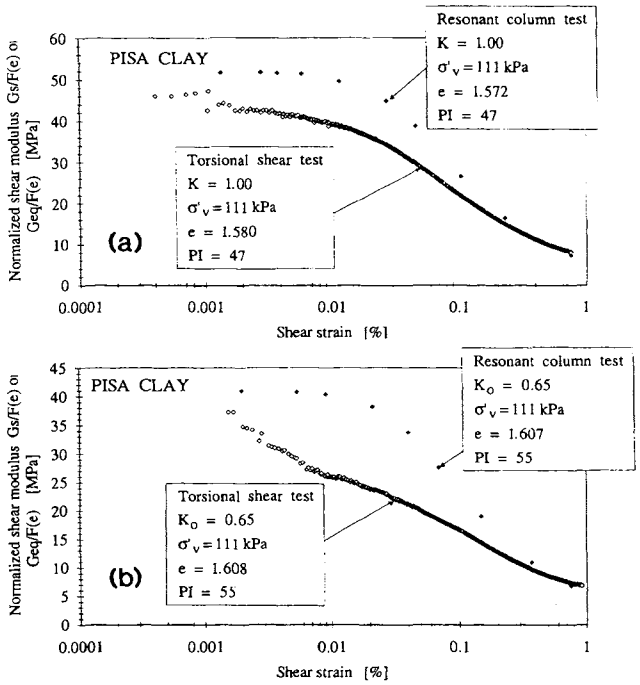

Fig. 45 Comparison of shear modulus and shear strain relations of Pisa clay from a static ML drained torsional shear test and a subsequently performed undrained torsional resonant-column test; the specimens were 5 cm OD, 3 cm in ID and 10 cm in H; $F(e)= e^{1.3}$ (Lo Presti, 1993).

DAMPING RATIO

General: The damping ratio measurement of geomaterials is in general more difficult than the stiffness measurement. Moreover, the damping ratio is affected by several factors more sensitively than the stiffness. These factors are the strain rate, the drainage conditions, the number of loading cycles, cyclic prestraining at a larger strain and so on. For this reason, the damping ratios of a given geomaterial obtained from different laboratories and different testing methods are often not consistent to each other. The effects of these factors are herein examined to some extent.

Effects of strain rate and drainage condition: The result of the round robin test program using Toyoura sand showed that under fully drained and undrained conditions, at relatively slow strain rates, the damping ratio (h value) is essentially independent of the drained conditions at strains of less than about 0.01 %, where the effective mean stress does not change largely during one undrained loading cycle. Furthermore, a noticeable effect of the strain rate on the h value was not observed in the cyclic triaxial tests on Toyoura sand for which the E_{eq} values are presented in Fig. 40.

Common for all geomaterials, due to non-linear deformation properties, the h value increases with the increase in the strain amplitude $(\varepsilon_a)_{SA}$. On the other hand, the h~strain rate relations obtained from undrained and "drained" cyclic triaxial loadings on sedimentary soft mudstone depend largely on both the drainage condition and the strain rate (**Fig. 46**). The effects of these two factors are equivalent to, or even larger than, the effects of strain non-linearity. This behaviour should be understood as follows;

1) Due to the creep deformation properties of the

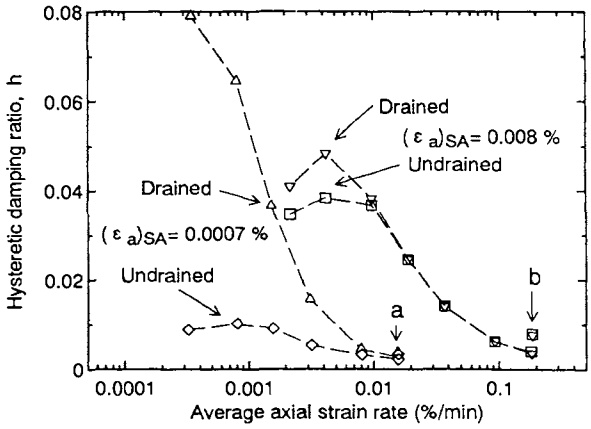

Fig. 46 Effect of strain rate on damping ratio in drained and undrained cyclic triaxial tests on sedimentary soft mudstone from Sagamihara site (Kohata et al., 1994b).

mudstone, under undrained conditions, the h value increases with the decrease in the strain rate (**Fig. 47**).

2) When a test specimen is under drainage conditions, the pore water moves relative to the geomaterial skeleton during each cycle according to the elastic volumetric deformation of the geomaterial skeleton caused by the change in the effective mean pressure (plus some amount of dilatancy when shear strains are larger than about 0.01 %); i.e., the pore water tends to be drained from and sucked into a test specimen when the axial stress increases and decreases, respectively. Therefore, energy is dissipated by the friction between the pore water and the surface of the geomaterial skeleton. The frictional stress becomes smaller as the strain rate decreases. At sufficiently low strain rates, the sample is fully drained in a "drained" test with nearly zero effect of the friction,

in which the excess pore water pressure is nearly zero throughout the specimen. In a "drained" test in which the sample is partially drained, however, the h value becomes larger than that observed under undrained conditions. This point can also be seen from Figs. 42; the hysteresis loops of the "drained" tests (Fig. 42 a and c) are larger than those of the undrained tests (Figs. 42 b and d), in particular at smaller strain rates. This factor can be explained in another way referring to **Fig. 48**. The solid and broken lines represent the stress-strain relations of a water-saturated porous linear elastic material measured by cyclic triaxial tests at a constant lateral stress, respectively, under fully undrained conditions (at any strain rate) and under fully drained conditions at a sufficiently low strain rate with zero effect of the frictional stress between the pore water and the elastic material skeleton. For the two relations, the h value is zero. When cyclic deviator stresses (Fig. 48a) are applied under partially drained conditions, the stress-strain curve is located in-between these two relations with h= 0.0, which leads to an increase in the hysteresis loop area.

3) It can also be seen from Fig. 46 that the difference in the h value between the "drained" and undrained tests increases as the strain rate decreases (see also Fig. 42). This tendency should be explained as follows. As the strain rate decreases, the specimen becomes more drained (i.e., the amount of moving pore water per cycle becomes larger) and the creep deformation becomes larger, by which the h value increases, while the frictional stress decreases, by which the h value decreases. For the range of strain rate examined in this test, as the strain rate decreases, the effects of the first two factors becomes larger than the effect of the last factor. It is very interesting to note in Fig. 46 that under "drained" conditions, even at a very small strain ($\varepsilon_a)_{SA}$= 0.0007 %, the h value becomes as large as 8 %. However, for a certain range of strain rates which are lower than the lowest strain rate examined in this test, the h value in the "drained" test should decrease as the strain rate decrease. For a sufficiently large range of strain rate, therefore, the h value in a "drained" test should have a maximum at a certain strain rate.

4) In Fig. 46, the data points denoted by the letter b stand for the h values obtained after all the other cyclic tests at ($\varepsilon_a)_{SA}$= 0.008 % had been performed (see Fig. 41). These h values are noticeably larger than the corresponding values obtained before a series of cyclic loadings were applied at different strain rates for ($\varepsilon_a)_{SA}$= 0.008 %. This increase in the h value may be due to the effect of a sort of deterioration of, or damage to, the structure, as seen from a slightly smaller E_{eq} value for the data points b (Fig. 41). Such an effect was not observed at ($\varepsilon_a)_{SA}$= 0.0007 % (see data points denoted by the letter a in Figs. 41 and 46).

Fig. 49 shows the h values of Pleistocene clay (OAP clay) (see Fig. 44). In this case, the effect of partial drainage on the h value is very obvious for ($\varepsilon_a)_{SA}$= 0.005 %, while is less for ($\varepsilon_a)_{SA}$= 0.0005 %. The behaviour is generally similar to that for the sedimentary mudstone (Fig. 46), and a tendency of the maximum h value in the "drained" test can be noted. One more factor is necessary, however, to explain the whole behavior. That is, at strain rates larger than a certain value, the h value under undrained conditions increases with the increase in the strain rate. As this trend can be seen in undrained tests, this increase in the h value is not due to the frictional effects between the pore water and the clay particles, but may be due to the viscous effects caused by very local displacements of the pore water. It can be seen that in the undrained test,

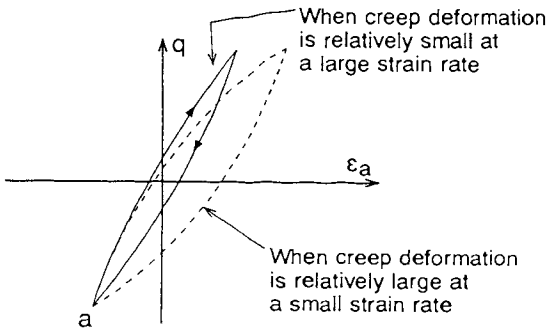

Fig. 47 Schematic figure to explain the creep effect on damping.

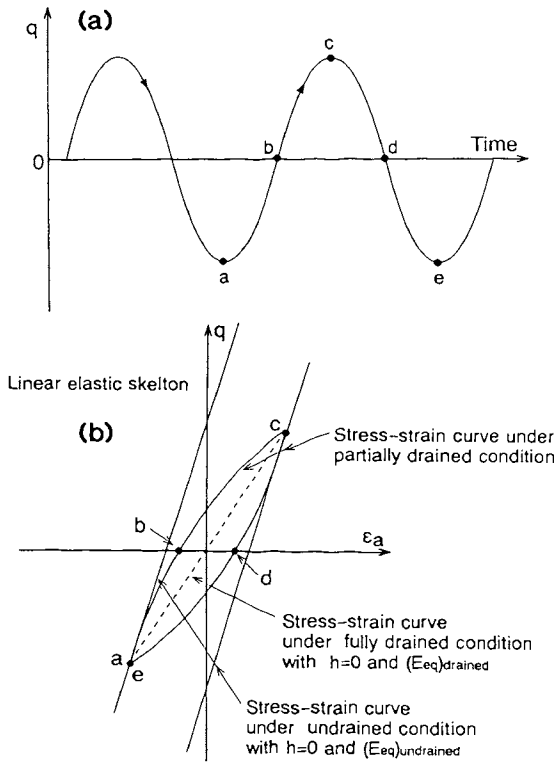

Fig. 48 Schematic figure to explain the effect of partial drainage on damping.

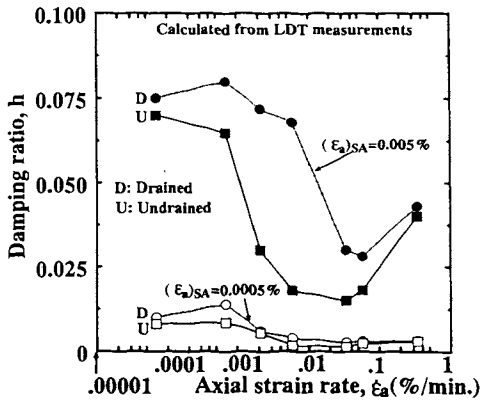

Fig. 49 Effect of strain rate on damping ratio in drained and undrained cyclic triaxial tests on Pleistocene clay (OAP clay) (tested by Mr. Mukabi,J.N., 1994).

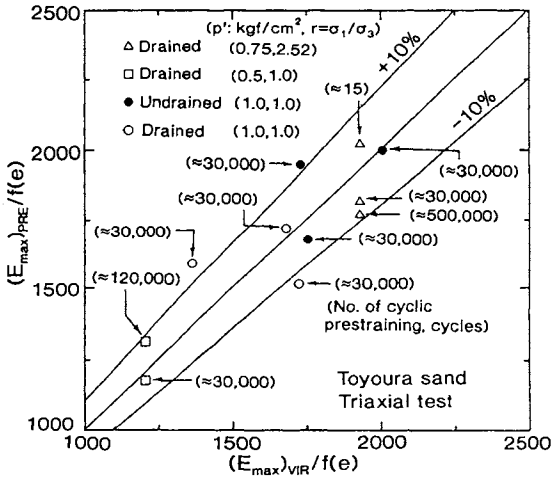

Fig. 50 Comparison of E_{max} values measured before and after the application of cyclic prestraining at $(\varepsilon_a)_{SA}$= 0.03 - 0.05 % in cyclic triaxial tests on Toyoura sand (Teachavorasinskun et al., 1992, 1994, Kohata et al., 1993).

the h value has a minimum at both $(\varepsilon_a)_{SA}$= 0.0005 % and 0.005 %. This behaviour is likely due to the balancing of viscous and creep effects. This is not the case with the undrained test result of sedimentary soft rock shown above, but this behaviour may be observed at higher strain rates. These points discussed above have also been discussed by Toki et al. (1994) and Shibuya et al. (1995).

It is not known if such effects of partial drainage on the h value have an engineering implication in the field. This effect could be noticeable when pore water moves relative to soil particles such as in a large submerged mass of large diameter particles subjected to seismic loading (e.g., rock fill dams). On the other hand, it seems that the effects of partial drainage on the h value would be very small in torsional shear tests in which the change in the mean pressure during each loading cycle is very small.

Summary; It can be seen from the above that the damping of geomaterials is more sensitive to several factors than the E_{eq} values. In the next section, it is also shown that damping ratio is much more sensitive than stiffness to the number of loading cycles at a fixed strain and cyclic prestraining applied at a strain larger than that at which the h value is measured.

EFFECTS OF CYCLIC PRESTRAINING

General; For a given mass of a geomaterial, if the elastic stiffness is not stable, for example, if it changes largely by cyclic straining applied at relatively small strains, it cannot be a basic parameter, since very different values can be easily obtained by using different testing methods. This would not be the case with geomaterials, however. On the other hand, other properties which are observed at strains exceeding the elastic limit strain, including damping, plastic deformation properties such as strain-non-linearity and dilatancy, and liquefaction properties, are less stable. These properties cannot, therefore, be evaluated only from the elastic stiffness.

Test results; It may be noted from Fig. 5 that by the application of cyclic straining at $(\varepsilon_a)_{SA}$= 0.02 % and 0.06 % for, respectively, dense and loose specimens of Toyoura sand, the $E_{eq} \sim (\varepsilon_a)_{SA}$ relation changed only very slightly. **Fig. 50** compares the E_{max} values measured

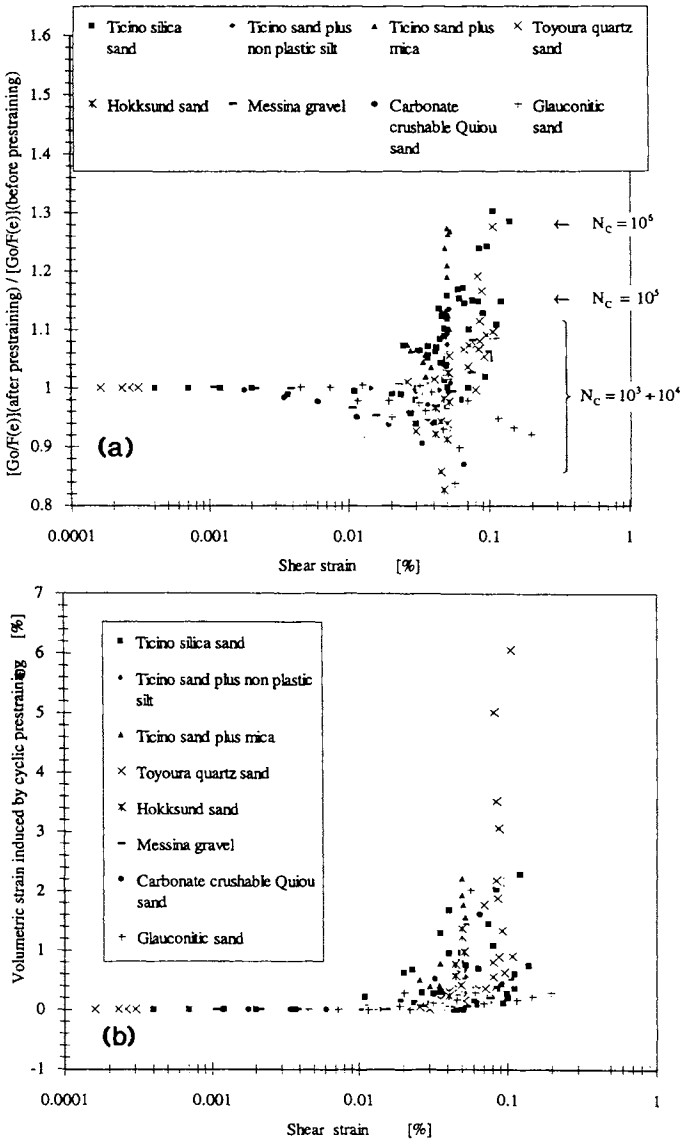

Fig. 51 a) G_{max} corrected for the density change and b) volumetric strain induced during cyclic prestraining, plotted against the strain applied during cyclic prestraining, obtained from torsional resonant-column tests of solid cylindrical specimens of 7.1 cm in D and 14.2 cm in H; $F(e)= (2.27 - e)^2/(1 + e)$ for Ticino sand, $(1.96 - e)^2/(1 + e)$ for Hokksund sand, $(2.18 - e)^2/(1 + e)$ for Glauconitic sand, $(1.32 - e)^2/(1 + e)$ for Messina gravel, $(4.60 - e)^2/(1 + e)$ for Ticino sand with Mica, $e^{1.3}$ for Quiou sand, $(2.17 - e)^2/(1 + e)$ Toyoura sand (Lo Presti, 1994).

before and after the application of cyclic prestraining obtained from these and similar other undrained and drained cyclic triaxial tests on Toyoura sand. The E_{max} values have been corrected for the change in the void ratio which occurred during cyclic prestraining by using the void ratio function $f(e)= (2.17 - e)^2/(1 + e)$ (n.b., the amount of correction was in fact small, particularly for the dense specimens). It may be seen that the E_{max} values have not changed noticeably by the application of cyclic prestraining. This is also the case with Ticino sand (Fig. 39) and gravel (Dong et al., 1994).

Figs. 51(a) and **(b)** show the effects of cyclic prestraining on G_{max} and volumetric strain induced during cyclic

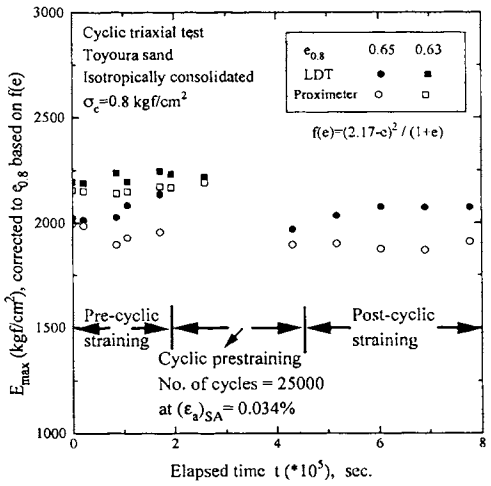

Fig. 52 Changes in E_{max} of air-pluviated air-dried Toyoura sand with consolidation time in cyclic triaxial tests; at an intermediate period, cyclic straining was applied at a larger strain (tested by Mr. Hoque,E., 1994).

prestraining obtained from a comprehensive series of torsional resonant-column tests (Lo Presti, 1994). Cyclic prestraining was applied for a number of cyclic load of as large as 1,000 to 1,000,000 at a shear strain up to a relatively large value of 0.2 %. It is interesting to note that due to cyclic prestraining, the G_{max} value either increases or decreases depending on the type of material. That is, Toyoura sand and Ticino sand exhibited the largest volumetric strain during cyclic prestraining at large strains and the largest increase in G_{max}. On the other hand, more crushable sands and gravels exhibited a smaller increase or a decrease in the G_{max} value by cyclic prestraining. In any case, however, the change in the G_{max} value is within as small as ± 25 %.

It has also been confirmed that for Toyoura sand and Ticino sand, the effect of consolidation time on the E_{max} is nearly the same before and after the application of cyclic prestraining at a larger strain, and the time effect is very small (**Fig. 52**). For the data shown in Fig. 52, two tests were performed, in which E_{max} values at $(\varepsilon_a)_{SA}$= about 0.001 % were measured periodically by applying ten cycles of symmetrical cyclic sinusoidal deviator stresses at a frequency of 0.1 Hz on an isotropically consolidated specimen of air-pluviated air-dried Toyoura sand. For one specimen, at an intermediate period, 25,000 cycles of cyclic loading was applied at $(\varepsilon_a)_{SA}$= 0.034 %. The plotted E_{max} values have been corrected to void ratios 0.65 and

Table 4 Effects of consolidation time on G_{max} before and after the application of cyclic prestraining (tested by Dr. Pallara, 1994).

Soil	G_{max}	e	$G_{max}/F(e)$	σ'_v	σ'_h	γ_p	N_c	t
-	[MPa]	-	[MPa]	[kPa]	[kPa]	[%]	-	[min.]
Quiou	51	0.898	44	51	51			
Quiou	46	0.884	39	51	51	0.063	10620	1
Quiou	50	0.884	43	51	51	0.063	10620	1470
Ticino	69	0.824	60	50	50			
Ticino	77	0.822	66	50	50	0.056	11205	1
Ticino	79	0.822	69	50	50	0.056	11205	15
Ticino	83	0.821	72	50	50	0.056	11205	1486
Toyoura	83	0.786	77	51	51			
Toyoura	94	0.784	87	51	51	0.053	10824	1
Toyoura	103	0.783	95	51	51	0.053	10824	1471

Where:

G_{max} = small strain shear modulus (γ = 0.0001-0.0003%)
e = void ratio
$G_{max}/F(e)$ = small strain shear modulus divided by the void ratio function
σ'_v = vertical consolidation stress
σ'_h = horizontal consolidation stress
γ_p = shear strain applied during prestraining
N_c = number of cycles during prestraining
t = time elapsed since the end of cyclic prestraining

Dry specimens

$F(e) = \frac{(2.27-e)^2}{(1+e)}$ Ticino sand

$F(e) = \frac{(2.17-e)^2}{(1+e)}$ Toyoura sand

$F(e) = e^{-1.3}$ Quiou sand

0.63 for the two tests, respectively. It may be noted that the E_{max} values are very stable with consolidation time both before and after the application of cyclic straining. A similar result was obtained also by a series of resonant-column tests on three types of sands (**Table 4**). It is very unlikely that the ageing effects increase after the application of cyclic prestraining.

One should note that the effect of cyclic prestraining is very large on the stress-strain relation at strains exceeding the elastic limit in triaxial compression tests on sand (Tatsuoka and Shibuya, 1992, Teachavorasinskun et al., 1994) and gravel (Kohata et al., 1994a, and Dong, 1994).

On the other hand, it can be seen from Fig. 5 that effects of cyclic prestraining on the h value is very large (see also **Figs. 53 a, b** and **c**). For the data shown in these figures, air-pluviated sand samples were isotropically consolidated to σ'_c = 50 kPa, and the h~$(\varepsilon_a)_{SA}$ relations were obtained first by following the test procedure used for the round robin test program. At the largest strain

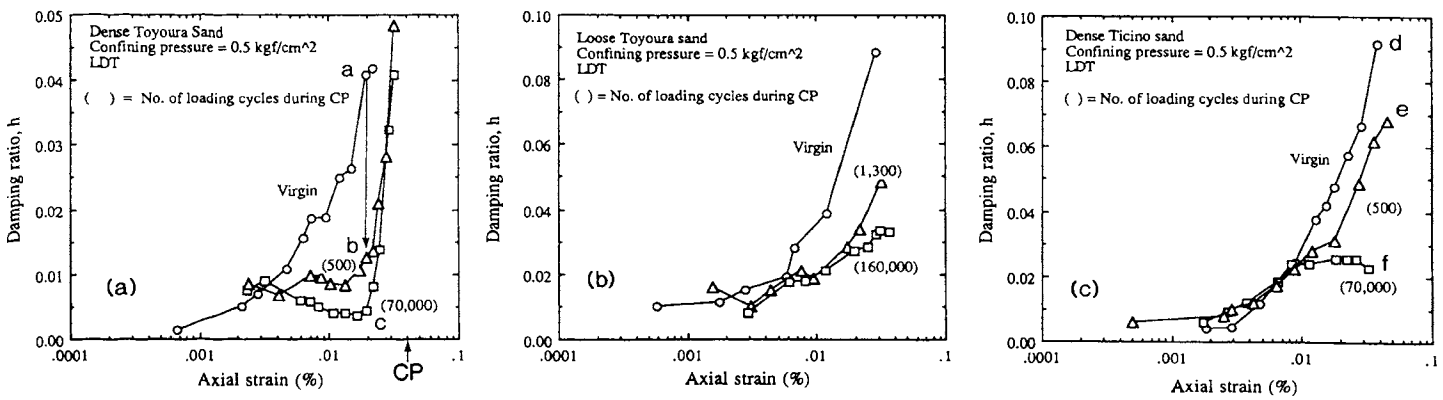

Fig. 53 Effects of cyclic loading on damping of air-pluviated sand samples in cyclic triaxial tests; a) dense Toyoura sand, b) loose Toyoura sand, and c) Ticino sand (Teachavorasinskun, 1992, Kohata et al., 1993).

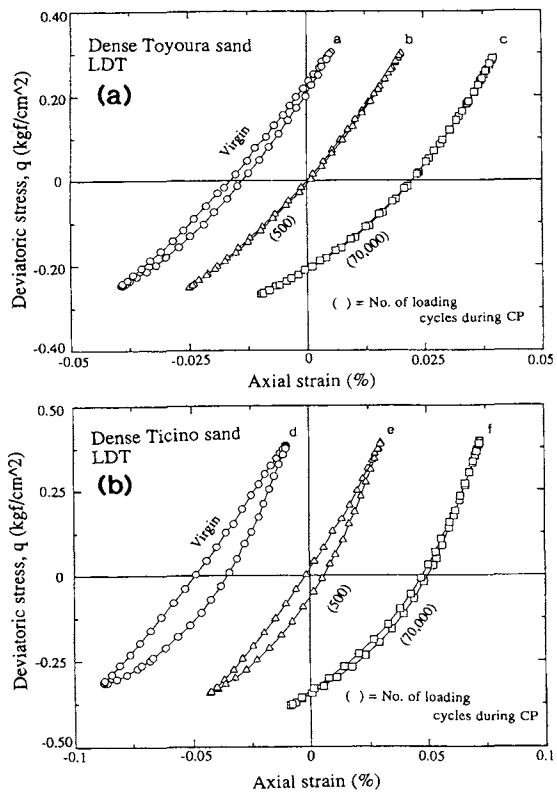

Fig. 54 Effects of cyclic loading on hysteresis loops of air-pluviated sand samples in cyclic triaxial tests; a) dense Toyoura sand (see Fig. 53a), b) Ticino sand (see Fig. 53c) (Teachavorasinskun, 1992, Kohata et al., 1993).

level for the first series of cyclic loading tests, then, cyclic deviator stresses were applied for the number of cycles indicated in the parenthesis in these figures. Subsequently, another series of cyclic loading tests were performed. For Toyoura sand and Ticino sand, respectively, three and two series of cyclic tests were performed for each specimen. The hysteresis loops at typical cyclic loading stages designated by the letters **a** to **f** in Fig. 53 are shown in **Fig. 54**. The following trends of behavior can be seen from Figs. 53 and 54:

1) The effect of cyclic prestraining on the h values decreases as the strain becomes smaller than that at which cyclic prestraining was applied; the data suggests that at strains $(\varepsilon_a)_{SA}$ close to the elastic limit strain, the effect is very small.

2) As the strain becomes closer to the value at which cyclic prestraining was applied, the effect becomes larger; a very large reduction can be noted in the h value measured after the application of cyclic prestraining. It can be seen from Fig. 54 that the peak-to-peak secant Young's modulus E_{eq} has not changed noticeably due to cyclic prestraining, but the hysteresis area has decreased substantially.

A similar result has been obtained for gravel (Dong et al., 1994). These results suggest that the damping ratio h decreases as the structure becomes more stable. It is, therefore, inferred, that the damping ratio becomes smaller also by the effect of ageing; perhaps, the damping ratio of a given aged soil in the field is smaller than that of the corresponding sample reconstituted in the laboratory measured under otherwise the same conditions.

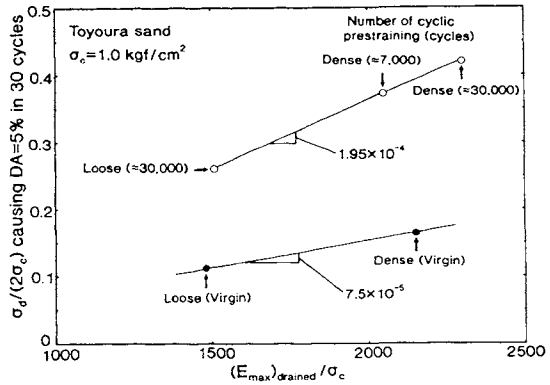

Fig. 55 Relationship between liquefaction strength and normalized maximum Young's modulus E_{max} for virgin and cyclically prestrained Toyoura sand (Teachavorasinskun et al., 1992, 1994).

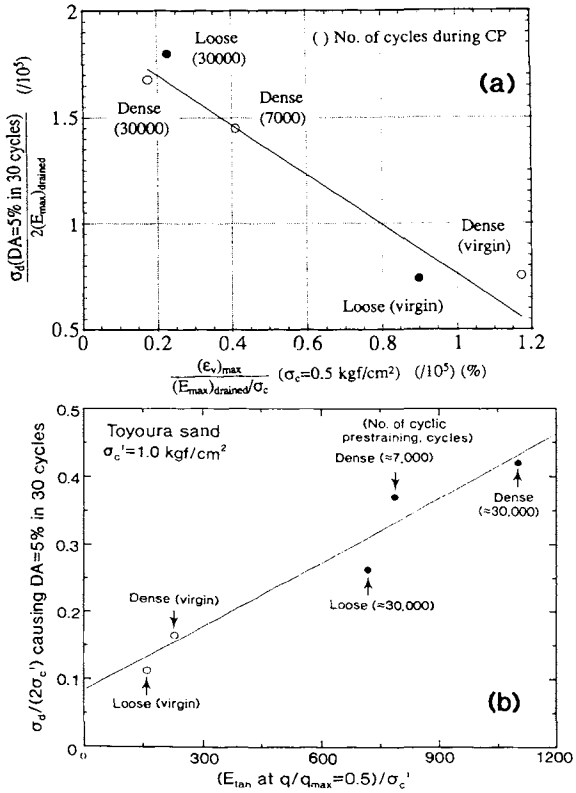

Fig. 56 Relationships between liquefaction strength and a) normalized maximum contractancy and b) normalized tangent Young's modulus E_{tan} at q/q_{max}= 0.5 for virgin and cyclically prestrained Toyoura sand (Teachavorasinskun et al., 1994).

Elastic stiffness and liquefaction strength: It is known that the resistance of saturated sand against undrained cyclic loading (i.e., liquefaction strength) increases considerably with the application of cyclic prestraining for which the E_{max} value hardly increases (Teachavorasinskun et al., 1992, 1994). **Fig. 55** shows the relationship between the liquefaction strength and the maximum drained Young's modulus E_{max} divided by σ_c' for virgin and cyclically prestrained samples of air-pluviated Toyoura sand isotropically consolidated to σ_c' = 98 kPa. These two quantities for each data point were measured for an identical sample. The liquefaction strength was defined as the cyclic stress ratio $\sigma_d/(2\sigma_c')$ (σ_d= single amplitude deviator stress) with which the double amplitude

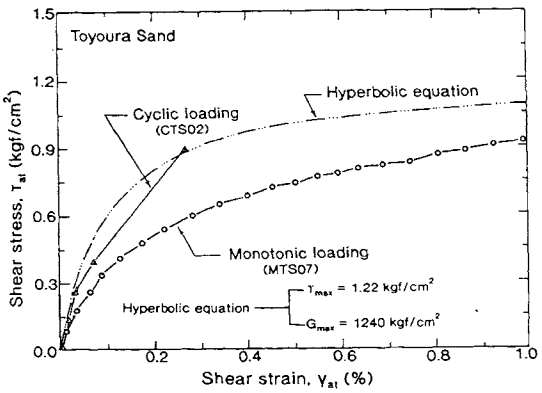

Fig. 57 Relationships between the single amplitude shear stress $(\tau)_{SA}$ and the single amplitude shear strain $(\gamma)_{SA}$ and between the shear stress τ and the shear strain γ, obtained from cyclic and monotonic, respectively, torsional simple shear tests on K_o consolidated Toyoura sand (Teachavorasinskun et al., 1991)

axial strain became 5 % in 30 cycles. It can be seen that the relation is utterly different between the virgin and cyclically prestrained specimens. That is, the liquefaction strength is not a unique function of the elastic Young's modulus E_{max}. This result suggests that it may not be possible to estimate the liquefaction strength of sand in the field only by the field shear wave velocity.

On the other hand, **Fig. 56(a)** shows the relationships between the liquefaction strength measured at σ_c' = 98 kPa and the normalized maximum contractancy obtained from drained triaxial compression tests performed at σ_c' = 49kPa on virgin and cyclically prestrained samples. For the same type of specimens used to obtain the liquefaction strength, the maximum contractancy was defined as the largest contractive volume strain attained until the peak stress state was reached in the drained triaxial compression test performed under the same test conditions except for the σ_c' value. **Fig. 56(b)** shows the relationship between the liquefaction strength measured at σ_c' = 98 kPa and the ratio of the tangent Young's modulus E_{tan} to σ_c'. The values of E_{tan} were defined for a shear stress level q at half of the peak strength q_{max} in the drained triaxial compression tests performed at σ_c' = 49 kPa on virgin and cyclically prestrained samples. This value was converted to that at σ_c' = 98 kPa by assuming that the ratio E_{tan}/E_{max} at a given q/q_{max} is independent of σ_c' under otherwise the same conditions. It can be seen that the liquefaction strength is closer linked to these two types of deformation properties measured at strain levels far exceeding the elastic limit strain.

Summary: Elastic stiffness is much more stable than the plastic deformation properties. Therefore, elastic deformation properties can be one of the generic parameters of a given geomaterial under given stress and strain states. It is known that by the change in some factors such as density and ageing, the liquefaction potential of a saturated sand deposit increases as the E_{max} or G_{max} value does. It should be noted, however, that the liquefaction potential, as well as the other plastic deformation properties observed at strains exceeding the elastic limit strain including the damping ratio and the decay properties of stiffness, cannot be estimated based only on the elastic deformation properties. Another parameter (or other parameters) representing plastic deformation properties in-situ, other than field shear wave velocity, should be determined by some appropriate field and/or laboratory tests.

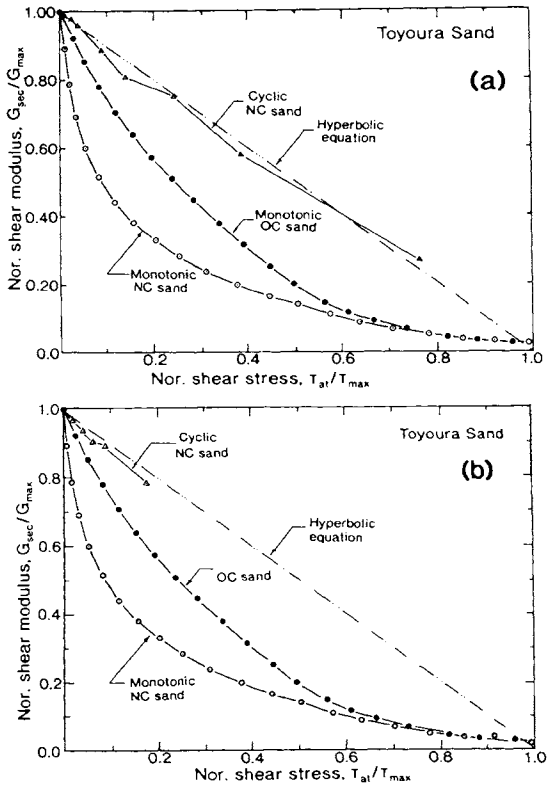

Fig. 58 Relationships between the ratio G_{eq}/G_{max} and the ratio of the single amplitude shear stress $(\tau)_{SA}$ to the peak shear stress τ_{max} and between the ratio G_{eq}/G_{max} and the ratio of the shear stress τ to the peak stress τ_{max}, obtained from cyclic and monotonic, respectively, torsional simple shear tests on K_o consolidated Toyoura sand (Teachavorasinskun et al., 1991)

STRAIN-DEPENDENCY OF STIFFNESS

Test results: Although almost the same elastic stiffness can be evaluated by ML and CL tests, the decay curves ($E\sim\varepsilon_a$ and $G\sim\gamma$ curves) can be very different. In drained (torsional) simple shear tests (Figs. 35 and 38), this difference is essentially due to the cyclic strain hardening effect, but only partly due to the different degrees of densification which occurred during the ML and CL tests. **Figs. 57** and **58**, which correspond to Fig. 35, show the cyclic strain hardening effect in other forms of plotting. One should note that this effect of cyclic strain hardening devalues the use of Masing's second rule.

Even for torsional shear tests, the relationship between the decay curves from ML and CL tests is made complicated by not only the strain hardening effect, but also other factors. **Fig. 59** shows the relationships between the ratio G_{eq}/G_{max} and the ratio of the single amplitude shear stress $(\tau)_{SA}$ to the peak shear stress τ_{max} and those between the ratio G_{eq}/G_{max} and the ratio of the shear stress τ to the peak stress τ_{max}, obtained from, respectively, cyclic and monotonic torsional shear tests on isotropically consolidated Ticino sand. It is seen from Fig. 59 (and also from Fig. 58) that by the effects of mechanical over-consolidation and cyclic prestraining, the decay curves from a ML test becomes similar to that from the corresponding CL test. It can be seen that the classical hyperbolic relation is only a crude approximation for the actual behaviour.

A comparison of the decay curve between a triaxial compression test and a cyclic triaxial test, both performed at a constant confining pressure, as seen in Figs. 4, 15a and 38, is much more complicated than that of (torsional) simple shear tests. This point is discussed based on the test results shown in Fig. 38. The following trends can be noted;
1) As the strain increases, the decay curves obtained from the triaxial compression test and cyclic triaxial test become more different, but the difference is smaller than that between the monotonic and cyclic torsional shear tests.
2) The decay is smaller in the triaxial compression test than in the ML torsional shear test.
3) The decay is larger in the cyclic triaxial test than in the CL torsional shear test.

These phenomena can be explained as follows. In a triaxial compression test at a constant confining σ_r pressure on sand, the increase in the axial stress results in an increase in the elastic Young's modulus defined in the axial loading direction (Kohata et al., 1994, Tatsuoka and Kohata 1995). This is a factor which decreases the rate of the decrease in the secant Young's modulus E_{sec} with the increase in the strain; this factor may even increase the E_{sec} value with the increase in the strain for very stiff gravels (Kohata et al., 1994). This factor (factor 1) is not involved in the ML and CL torsional shear tests. On the other hand, in the cyclic triaxial test with symmetric cyclic deviator stresses, the axial stress σ_a decreases when loaded in triaxial extension with the maximum stress ratio $\sigma_1/\sigma_3=\sigma_r/\sigma_a$ being much larger than the minimum stress ratio $\sigma_1/\sigma_3=\sigma_a/\sigma_r$ in triaxial compression. This is a factor to decrease the stiffness E_{eq} (factor 2). When the effect of the factor 2 overwhelms the effect of cyclic strain hardening, the rate of the decrease in the E_{eq} with the increase in the strain in a cyclic triaxial test can become larger than that in the corresponding triaxial compression test involving the effect of the factor 1. This is the case with a very dense well-graded gravel with high stiffness relative to the strength in triaxial extension (see Fig. 15a). It should also be noted that a good coincidence for a wide range of strains between the decay curves from drained cyclic triaxial and cyclic torsional shear tests is fortuitous. Their relationship primarily depends on the stiffness of the soil. Therefore, a decay curve obtained from a drained cyclic triaxial test performed at a constant confining pressure should be applied with a caution to drained cyclic simple shear conditions.

For the saturated clays, decay curves obtained by a staged undrained cyclic triaxial test in which a sample is drained between successive undrained loading stages and the corresponding CU triaxial compression test are often similar. **Fig. 60** shows a case typical of the above. This agreement can be obtained particularly when the degree of strain softening due to the increase in the pore water pressure is small in the undrained cyclic loading test and the change in the mean effective principal stress is small during the CU triaxial compression test. This is the case of sedimentary soft mudstone (Fig. 22) and cement-treated soils (Shibuya et al., 1992). One should note, however, that the relationship between the decay curves from static tests and resonant-column tests becomes more complicated due to the effects of variable strain rates in the latter type of test (see Fig. 45) (Isenhower and Stokoe, 1981).

In this report, the effects of long-term consolidation, density, inherent anisotropy, stress system-induced anisotropy, shear strain-induced anisotropy and other factors on the stiffness and damping ratio were not touched, but they are discussed to some extent in

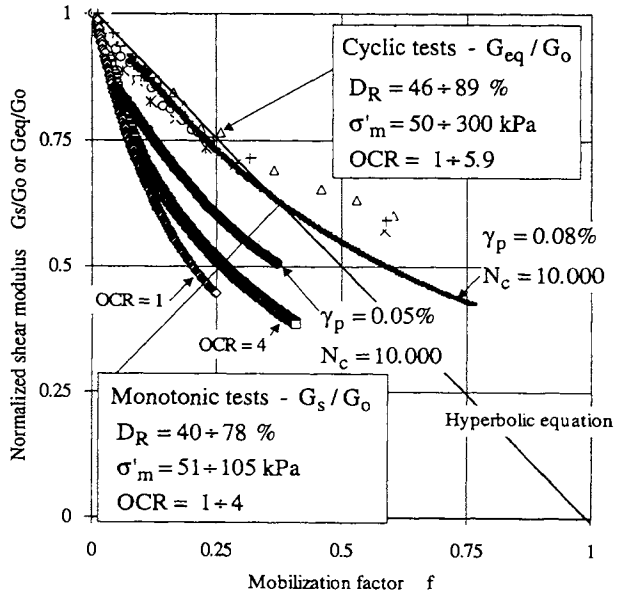

Fig. 59 Relationships between G_{eq}/G_{max} and $f=(\tau)_{SA}/\tau_{max}$ and between G_{eq}/G_{max} and $f=\tau/\tau_{max}$, obtained from cyclic and monotonic, respectively, torsional shear tests on isotropically consolidated Ticino sand (Lo Presti et al., 1993)

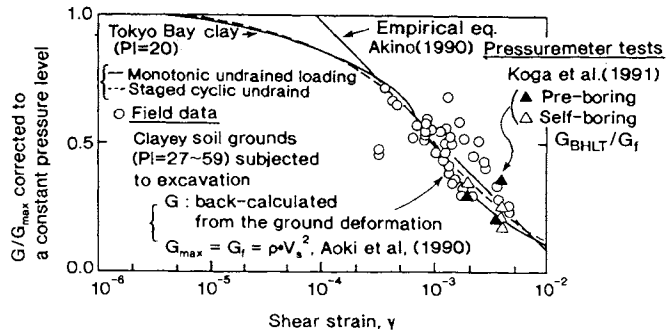

Fig. 60 Comparison of shear moduli from field and laboratory tests and those from full-scale field behavior for clay deposits (Tatsuoka, 1991).

Tatsuoka and Shibuya (1992) and Tatsuoka and Kohata (1995).

Engineering Implications: The data points shown in Fig. 60 are; 1) the shear moduli G_{sec} back-calculated from a number of full-scale field behavior of clay deposits observed during ground excavation and construction of high-rise buildings (Aoki et al., 1990) divided by the elastic shear modulus G_T obtained from the field shear wave velocities, and 2) the shear modulus G_{BHLT} obtained from pressuremeter tests evaluated based on the conventional linear theory divided by G_T (Koga et al., 1991). A good agreement between the laboratory and field data may be noted.

Based on this and a great deal of similar experience (Tatsuoka and Kohata, 1995), the following methodology can be suggested to estimate the decay curve not only for dynamic and static CL problems (**Fig. 61a**), but also for static ML loading problems (**Fig. 61b**), that is;
1) First, the value of G_T is estimated by field seismic surveys.
2) Appropriate laboratory stress-strain tests are

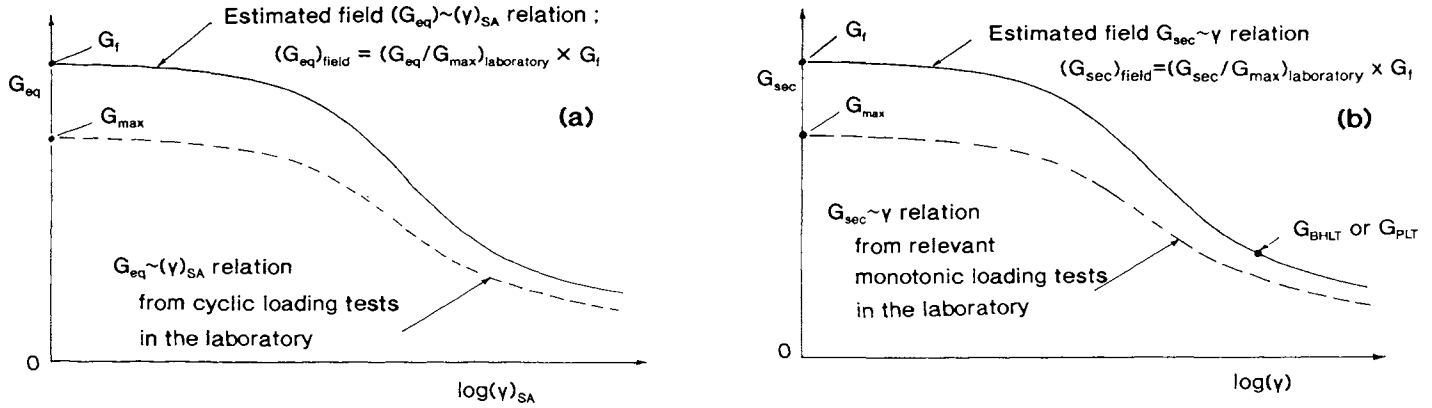

Fig. 61 A suggested method to estimate the in-situ stiffness as a function of strain (Tatsuoka and Shibuya, 1992)

performed using high-quality undisturbed samples. The quality of the sample is evaluated by comparing the maximum shear modulus G_{max} from the laboratory tests with the corresponding G_f value.
3) The field decay curve is estimated by taking into account the strain level-dependency (strain non-linearity), the pressure level-dependency (or more generally, the effects of stress path during loading), and the effects of cyclic loading (if necessary), the drainage condition, strain rate, previous strain history and so on. In so doing, the G_f value is selected as the average maximum shear modulus in the field, while considering the effect of the pressure change on it if necessary.
4) If possible, the estimated field decay curve is calibrated by the results of pressuremeter tests and/or plate loading tests.

CONCLUSIONS

The following conclusions can be derived from the data shown in this report:
1) For a wide range of geomaterials, in particular relatively stiff ones such as hard soils and soft rocks, in triaxial tests to be performed to accurately estimate the deformation characteristics at very small to small strains, the use of a load cell within the triaxial cell and a local axial strain gage along the specimen lateral surface is imperative.
2) With the use of an internal load cell and a local strain gage which are sufficiently sensitive, a continuous stress-strain relation for a strain range from less than 0.001 % to several % can be obtained from a single test using a single specimen.
3) For a deposit of soils and soft rocks, if test samples are not disturbed, the maximum shear modulus G_{max} measured at strains of less than 0.001 % obtained from laboratory stress-strain tests (e.g., triaxial tests) is very similar to the corresponding elastic shear modulus G_f obtained from field shear wave velocity.
4) For a wide variety of geomaterials, the deformation characteristics at strains of less than about 0.001 % are essentially elastic, whereas the stiffness becomes more strain rate-independent as the strain level decreases, particularly at strains of less than about 0.001 %. Therefore, at very small strains (or strain amplitudes), of smaller than about 0.001 %, a very similar stiffness can be obtained from static monotonic and cyclic loading tests and dynamic tests.
5) The damping ratio of geomaterials is more difficult to measure and is affected by several factors more sensitively than the stiffness. These factors include strain rate, drainage conditions, the number of loading cycles, cyclic prestraining at a larger strain. For this reason, much less is understood about the damping ratio than about the stiffness.
6) The cyclic undrained strength of saturated sand can increase considerably by the application of cyclic prestraining by which the E_{max} value does not exhibit a noticeable change. Therefore, the liquefaction potential of a given sand deposit is difficult to estimate based solely on field shear wave velocity.
7) The relationships between the decay curves obtained from a pair of drained monotonic and cyclic triaxial tests performed at a constant confining pressure depends largely on the stiffness relative to the strength in triaxial extension. In drained (torsional) simple shear tests on sand, the decay becomes smaller in a cyclic loading test than the corresponding monotonic loading test due to the effect of cyclic strain hardening. The decay curve could be similar between undrained ML and CL triaxial tests on clays. As the decay curve at large strains is strongly affected by the strain rate, in particular for cohesive soils, the decay becomes smaller in resonant-column tests, in which the strain rate increases nearly proportionally with the strain amplitude.
8) The stiffness at relatively small strains of a given geomaterial to be used to estimate full-scale field behavior of geotechnical structures, not only in soil dynamics problems, but also in static loading problems, can be estimated based on field shear wave velocities while taking into account the effects of any influencing factors.

In short, the elastic stiffness at very small strains is one of the most important key parameters for site characterization. At the same time, the plastic deformation characteristics observed at strains exceeding the elastic limit, which include the damping ratio, the liquefaction potential and the decay properties of stiffness, cannot be estimated based solely on the elastic deformation characteristics, but another parameter, or other parameters, in the field should be evaluated.

ACKNOWLEDGEMENT

The authors gratefully acknowledge the help and cooperation provided by their previous and current colleagues in preparing this report; at Institute of Industrial Science, University of Tokyo, Dr. Teachavorasinskun,S., Mr. Mukabi,J.N., Dr. Dong,J., Mr. Hoque,E., Mr. Suzuki,M., Mr. Sato,T. and Miss Torimitsu,M, and at Politecnico di Torino, Dr. Pallara,O., Mr. Maniscalco,R. and Mr. Impavido,M.

REFERENCES

Abbreviations used in the following:

ASCE; American Society of Civil Engineers
ASTM; American Society for Testing and Materials
GE; Geotechnical Engineering
GTJ: Geotechnical Testing Journal, ASTM
IIS: Institute of Industrial Science
IS-Hokkaido '94: International Symposium on Prefailure Deformation Characteristics of Geomaterials, Sapporo, September, 1994 (Shibuya et al., eds.)
JSSMFE; Japanese Society of Soil Mechanics and Foundation Engineering
S&F: Soils and Foundations, Journal of the JSSMFE

Aoki,M., Shibata,Y. and Maruoka,M. (1990), "Estimation of ground deformation during construction period (part 1)", Proc. Annual Conf. of Architecture Institute of Japan, Vol.B, pp.1649-1650 (in Japanese).

Armandi, M. (1991), "Caratteristiche di Deformabilita della Sabbia del Ticino e di Toyoura da Prove di Taglio Torsionale e Colonna Risonante", M. Sc. Thesis, Department of Structural Engineering, Politecnico di Torino.

Burland, J.B. (1989), "Ninth Laurits Bjerrum Memorial Lecture, "Small is beautiful" -the stiffness of soils at small strains", Canadian Geotechnical Journal, 26, pp.499-516.

Clayton,C.R.I. and Khatrush,S.A. (1986), A new device for measuring local axial strains on triaxial specimens, Geotechnique, 35, pp.62-65.

Dong,J., Nakamura,K., Tatsuoka,F., and Kohata,Y. (1994), "Deformation characteristics of gravels in triaxial compression tests and cyclic triaxial tests", Proc. Hokkaido '94, Balkema, Vol.I, pp.17-23.

Goto,S., Tatsuoka,F., Shibuya,S., Kim,Y.S. and Sato,T. (1991), "A simple gauge for local small strain measurements in the laboratory", S&F, 31-1, pp.169-180.

Fioravante V., Jamiolkowski M., Lo Presti D.C.F. and Pallara O. (1993), Discussion on "Elastic Deformation Properties of Geomaterials by Shibuya et al.,", S&F, 33-4, pp.194-197.

Hardin,B.O. and Richart,F.E. (1963), "Elastic wave velocities in granular soils", Jour. ASCE, 89-1, pp.33-65.

Hardin,B.O. and Black,W.L. (1968), "Vibration modulus of normally consolidated clay", Jour. of SMFE Div., Proc. ASCE, 94-SM2, pp.353-369.

Hardin,B.O. and Drnevich,V.P. (1972a), "Shear modulus and damping in soils: Measurement and parameter effects", Jour. of SMF Div., Proc. ASCE, 98-SM6, pp.603-624.

Hight,D.W. and Higgins,K.G. (1995), "An approach to the prediction of ground movements in engineering practice: background and application", Proc. IS-Hokkaido '94, Balkema, Vol.II.

Isenhower,W.M. and Stokoe,K.H.II. (1981), "Strain rate-dependent shear modulus of San Francisco Bay mud", Proc. INt. Conf. on Recent Advances in Geotechnical Earthquake Engineering and Soil Dynamics, St. Louis, MO, Vol.II, pp.597-602.

Iwasaki,T., Tatsuoka,F. and Takagi,Y. (1978), "Shear moduli of sands under cyclic torsional shear loading", S&F, 18-1, pp.39-56.

Jamiolkowski,M., Lerouell,S., and Lo Presti,D.C.F. (1991), "Design parameters from theory to practice", Theme Lecture, Geo-Coast '91, Yokohama, pp.877-917.

Jamiolkowski M., Lancellotta R., Lo Presti D.C.F., and Pallara O. (1994), "Stiffness of Toyoura Sand at Small and Intermediate Strain", Proceedings of the XIII ICSMFE, New Delhi, India, Vol I, pp.169-172.

Jardine,R.J., St.John,H.D., Hight,D.W. and Potts,D.M. (1991), "Some practical applications of a non-linear ground model", Proc. of 10th European Regional Conf. on SMFE, Firenze, I, pp.223-228.

Jardine,R.J. (1995), "One perspective of the pre-failure deformation characteristics of some geomaterials", Proc. IS-Hokkaido '94, Balkema, Vol.II.

Kim,Y.-S., Tatsuoka,F. and Ochi,K. (1994), "Deformation characteristics at small strains of sedimentary soft rocks by triaxial compression tests", Geotechnique, 44-3, pp.461-478.

Koga,Y., Matsuo,O. and Sugawara, N. (1991), "On estimating the moduli of ground by pressuremeter tests", Proc. Japan National Conf. on SMFE, Nagoya, Vol.I, pp.203-206 (in Japanese).

Kohata,Y., Tatsuoka,F., Teachavorasinskun,S., and Dong,J. (1993), "Damping characteristics of geomaterials in laboratory soil tests", Seisan Kenkyu, Jour. of IIS, 45-8, pp.3-10 (in Japanese).

Kohata,Y. Tatsuoka,F., Dong J., Teachavorasinskun,S. and Mizumoto,K. (1994a), "Stress-state affecting elastic deformation moduli of geomaterials", Proc. IS-Hokkaido '94, Balkema, Vol.I, pp.3-9.

Kohata,Y., Suzuki,M. and Tatsuoka,F. (1994b), "Deformation characteristics of geomaterials from cyclic and monotonic loading triaxial tests", Seisan Kenkyu, Jour. of IIS, 46-10, pp.3-9 (in Japanese).

Kokusho,T. (1980), "Cyclic triaxial test of dynamic soil properties for wide strain range", S&F, 20-2, pp.45-60.

Kokusho,T., Yoshida,Y. and Esashi,Y. (1982), "Dynamic properties of soft clay for wide strain range", S&F, 22-4, pp.1-18.

Lo Presti,D.C.F. (1987), "Mechanical Behaviour of Ticino Sand from Resonant Column Tests", Ph D. Thesis, Department of Structural Engineering, Politecnico di Torino.

Lo Presti,D.C.F. (1989), "Proprieta' dinamiche dei terreni", XIV CGT, Department of Structural Engineering, Politecnico di Torino.

Lo Presti,D.C.F., Pallara,O., Lancellota,R., Armandi,M. and Maniscalco,R. (1993), "Monotonic and Cyclic Loading Behaviour of Two Sands at Small Strains", GTJ, 16-4, pp.409-424.

Lo Presti,D.C.F., Pallara,O., Raino,M. and Maniscalco,R. (1994a), "A computer-controlled triaxial apparatus: preliminary results", Rivista Italiana di Geotecnica, Anno XXVIII,N.J., pp.43-60.

Lo Presti,D.C.F., Pallara,O., Costanzo,D., and Impavido,M. (1994b), "Small Strain Measurements During Triaxial Tests: Many Problems, some solutions", Proc. IS-Hokkaido '94, Balkema, Vol.I, pp.11-16.

Lo Presti,D.C.F. (1995), "Measurement of Shear Deformation of Geomaterials from Laboratory Tests", General Report for Session 1a, Proc. IS-Hokkaido '94, Balkema, Vol.II.

Lo Presti,D.C.F., Jamiolkowski,M., Pallara,O., Psiciotta V., and Ture S. (1995), "Stress dependence of sand stiffness", Proc. Third Int. Conf. on Recent Advances in Geotech. Earthquake Engineering and Soil Dynamics, St. Louis., MO.

Mukabi,J.N., Tatsuoka,F., Kohata,Y. and Akino,N. (1994), "Small strain stiffness of Pleistocene clays in triaxial compression", Proc. IS-Hokkaido '94, Balkema, Vol.I, pp.189-195.

Mukabi,J.N. (1994), Internal reports of IIS, Univ. of Tokyo and personal communications.

Ochi,K., Tatsuoka,F. and Tsubouchi,T. (1993), "Stiffness of sedimentary soft rock from in situ and laboratory tests and field behaviour", Geotechnical Engineering of Hard Soils-Soft Rocks (eds. Anagnostopoulos et al.), Balkema, 1, pp.707-714.

Ochi,K., Tsubouchi,T. and Tatsuoka,F. (1994), "Deformation characteristics of sedimentary soft rock evaluated by full-scale excavation", Proc. IS-Hokkaido '94, Balkema, Vol.I, pp.601-607.

Pallara O. (1995), "Stress-strain behaviour of two sands under monotonic and cyclic loading conditions", Ph. D. Thesis, Department of Structural Engineering,

Politecnico di Torino.
Park,C.-S. and Tatsuoka,F. (1994), "Anisotropic strength and deformation of sands in plane strain compression", Proc. of the 13th Int. Conf. on SMFE, New Delhi, 1, pp.1-6.
Shibuya,S., Tatsuoka,F., Teachavorasinskun,S., Kong,X.-J., Abe,F., Kim,Y.-S., and Park,C.-S. (1992), "Elastic deformation properties of geomaterials", S&F, 32-3, pp.26-46.
Shibuya,S., Mitachi,T., Fukuda,F. and Degoshi,T. (1995), "Strain rate effects on shear modulus and damping of normally consolidated clay", GTJ (to appear).
Tatsuoka,F. (1991), Panel discussion on "measurement of static deformation moduli in dynamic tests" (Session 1), Proc. 10th European Regional Conf. on SMFE, Florence, 1991, Post Conference Volume.
Tatsuoka, F. and Shibuya,S. (1992), "Deformation characteristics of soils and rocks from field and laboratory tests", Proc. 9th Asian Regional Conf. on SMFE, Bangkok, Vol.2, pp.101-170.
Tatsuoka,F., Teachavorasinskun,S., Dong,J., Kohata,Y. and Sato,T. (1994a), "Importance of measuring local strains in cyclic triaxial tests on granular materials", Dynamic Geotechnical Testing: Second Volume, ASTM STP 1213 (Edelhar, Drnevich & Kutter eds.), pp.288-302.
Tatsuoka,F., Sato,T., Park,C.S., Kim,Y.S., Mukabi,J.N. and Kohata,Y. (1994b), "Measurements of elastic properties of geomaterials in laboratory compression tests", GTJ, ASTM, 17-1, pp.80-94.
Tatsuoka,F. and Kohata,Y. (1995), Stiffness of hard soils and soft rocks in engineering applications", Keynote Lecture, Proc. IS-Hokkaido '94, Balkema, Vol.II.
Tatsuoka,F., Kohata,Y.,Tsubouchi,T., Murata, K., Ochi,K. and Wang,L. (1995), "Disturbance in rotary core tube sampling", Proc. Int. Conf. on Advances in Site Investigation Practice, the Institute of Civil Engineers, March, London.
Teachavorasinskun,S. (1992), "Stress-strain and strength characteristics of granular materials in simple shear", Dr. of Engineering Thesis, University of Tokyo.
Teachavorasinskun,S., Shibuya,S. and Tatsuoka,F. (1991), "Stiffness of sands in monotonic and cyclic torsional shear", Proc. Geotechnical Engineering Congress, 1991, ASCE Geotechnical Special Publication No.27 (eds. McLean et al.), Vol.II, pp.863-878.
Teachavorasinskun,S., Tatsuoka,F., Kenkyo,K. and Yasuhara,K. (1992), "Effect of cyclic prestraining on the liquefaction strength of sand", Proc. of on Behaviour of Offshore Structures Conf. (BOSS), London, 2, pp.1345-1356.
Teachavorasinskun,S., Tatsuoka,F., and Lo Presti, D.C.F. (1994), "Effects of cyclic prestraining on dilatancy characteristics and liquefaction strength of sand", Proc. IS-Hokkaido '94, Balkema, Vol.I, pp.75-80.
Toki,S., Shibuya,S. and Yamashita,S. (1995), "Standardization of Laboratory Test Methods to Determine the Cyclic Deformation Properties of Geomaterials in Japan", Keynote Lecture, Proc. IS-Hokkaido '94, Balkema, Vol.II.
Uchida,K., Shioi,Y., Hirukawa,T. and Tatsuoka,F. (1993), "The Trans-Tokyo Highway Project - A huge project currently under construction", Proc. of Int. Conf. on Transportation Facilities through Difficult Terrain (Wu and Barrett eds.), Balkema, pp.57-87.
Woods,R.D. (1991), "Field and laboratory determination of soil properties at low and high strains", SOA Paper, Proc. Second Int. Conf. on Recent Advances in Geotechnical Earthquake Engineering and Soil Dynamics, St. Louis, MO, Vol.II, pp.1727-1741.